Relaxation after quantum quenches in the spin-$\frac{1}{2}$ Heisenberg XXZ chain

Maurizio Fagotti,[1] Mario Collura,[2] Fabian H. L. Essler,[1] and Pasquale Calabrese[2]
[1]*The Rudolf Peierls Centre for Theoretical Physics, Oxford University, Oxford, OX1 3NP, United Kingdom*
[2]*Dipartimento di Fisica dell'Università di Pisa and INFN, 56127 Pisa, Italy*
(Received 26 November 2013; revised manuscript received 10 February 2014; published 3 March 2014)

We consider the time evolution after quantum quenches in the spin-$\frac{1}{2}$ Heisenberg XXZ quantum spin chain with Ising-type anisotropy. The time evolution of short-distance spin-spin correlation functions is studied by numerical tensor network techniques for a variety of initial states, including Néel and Majumdar-Ghosh states and the ground state of the XXZ chain at large values of the anisotropy. The various correlators appear to approach stationary values, which are found to be in good agreement with the results of exact calculations of stationary expectation values in appropriate generalized Gibbs ensembles. In particular, our analysis shows how symmetries of the post-quench Hamiltonian that are broken by particular initial states are restored at late times.

DOI: 10.1103/PhysRevB.89.125101 PACS number(s): 02.30.Ik, 05.70.Ln, 75.10.Jm, 67.85.−d

I. INTRODUCTION

Recent years witnessed great advances in our understanding of *isolated* nonequilibrium many-particle quantum systems, mainly triggered by ground-breaking experiments with ultracold, trapped atoms [1–5]. One of the most celebrated results is that expectation values of *local* observables generically approach stationary values at late times in the thermodynamic limit, in spite of the time evolution being unitary and the entire system concomitantly always being in a pure state (assuming that it started out in a pure state). There is compelling evidence that these stationary values can be predicted by statistical ensembles without having to solve the complicated nonequilibrium dynamics.

For nonintegrable models, the appropriate statistical ensemble is expected to be the standard Gibbs distribution with an effective temperature fixed by the value of the energy in the initial state [6]. For integrable models, the existence of *local* conservation laws strongly constrains the dynamics, and it has been proposed [7] that stationary values are described by a generalized Gibbs ensemble (GGE). By now, rather convincing evidence supporting this proposal has accumulated [8–27], but a general proof is still outstanding. Whereas in equilibrium integrability may be viewed chiefly as powerful tool for obtaining exact solutions of paradigmatic models, out of equilibrium it is an essential physical feature. For models that can be mapped to free fermions or bosons, the stationary behavior as well as essentially the full dynamics has been obtained analytically [10–14,17,25,26]. Unfortunately, the methods applicable to these cases do not generalize to *interacting* integrable models, i.e., models with momentum-dependent (dressed) scattering matrices.

A crucial next step is therefore to calculate expectation values of local observables in the stationary state after a quantum quench in interacting integrable models, assuming that local properties can be described by an appropriate GGE. This task has recently been undertaken by several groups using different integrability-based techniques [8,24,27–31]. In some of these works, specific predictions for stationary values of local observables have been made. Given the underlying assumption of relaxation to a GGE, these predictions need to be checked by independent methods such as numerical simulations.

Here, we focus on the nonequilibrium dynamics of the XXZ spin chain described by the Hamiltonian

$$H^{(1)}(\Delta)=\frac{1}{4}\sum_{\ell=1}^{L}\sigma_\ell^x\sigma_{\ell+1}^x+\sigma_\ell^y\sigma_{\ell+1}^y+\Delta\left(\sigma_\ell^z\sigma_{\ell+1}^z-1\right),\qquad \Delta=\cosh(\eta)>1. \tag{1.1}$$

We will consider a variety of initial states and consider the question as to whether the dynamics of local observables exhibits relaxation to a stationary state compatible with a GGE. The latter is of the form

$$\rho_{\rm GGE}=\frac{1}{Z_{\rm GGE}}\exp\left(hS^z-\sum_{l=1}\lambda_l H^{(l)}\right). \tag{1.2}$$

Here, $S^z=\frac{1}{2}\sum_\ell\sigma_\ell^z$ is the z component of total spin, $H^{(1)}$ is the Hamiltonian, and $H^{(l)}$ are local [11] integrals of motion that fulfill $[H^{(m)},H^{(n)}]=0$ and are obtained by taking logarithmic derivatives of the transfer matrix of the six-vertex model [32]. The Lagrange multipliers h and λ_l are fixed by the requirement that the expectation values of the conservation laws are the same at time $t=0$ and in the stationary state

$$\lim_{L\to\infty}\frac{\langle\Psi_0|S^z|\Psi_0\rangle}{L}=\lim_{L\to\infty}\frac{{\rm Tr}\,[\rho_{\rm GGE}S^z]}{L},\qquad \lim_{L\to\infty}\frac{\langle\Psi_0|H^{(l)}|\Psi_0\rangle}{L}=\lim_{L\to\infty}\frac{{\rm Tr}\left[\rho_{\rm GGE}H^{(l)}\right]}{L}. \tag{1.3}$$

We stress that locality of the integrals of motion is the key feature which sets integrable models apart from generic ones. In fact, *any* quantum mechanical Hamiltonian H has as many integrals of motions as there are basis states in the Hilbert space, as the one-dimensional projectors $P_n=|\psi_n\rangle\langle\psi_n|$ on energy eigenstates are in involution and commute with H. However, they are not local. The GGE built with all the P_n's is by definition equivalent to the so-called diagonal ensemble, which describes the infinite time average of arbitrary observables (including nonstationary ones) in a finite volume (assuming that spectral degeneracies do not play a role).

The last few months have witnessed considerable progress in developing analytic approaches to the quench problem in the XXZ spin chain [8,24,33–35]. In this paper, we follow the route developed by two of the present authors [8], which allows us to calculate short-distance spin-spin correlation functions in the appropriate GGEs. As compared to other methods, the approach of Ref. [8] works directly in the thermodynamic limit *at finite-energy density* compared to the ground state of the post-quench Hamiltonian. Here, we extend the calculations of Ref. [8] to a variety of initial states not previously considered. We also provide the details of how to treat initial states of matrix-product form, which may be known only numerically from a ground-state tensor network computation.

A. Symmetry restoration after quantum quenches

A key issue we will be investigating is that of *symmetry restoration*. The post-quench Hamiltonian exhibits a number of symmetries such as follows:

(1) U(1) rotations around the z axis in spin space:

$$\sigma_\ell^\pm \longrightarrow e^{\pm i\varphi}\sigma_\ell^\pm, \quad \sigma_\ell^\pm = \frac{\sigma_\ell^x \pm i\sigma_\ell^y}{2}. \tag{1.4}$$

(2) Translational invariance:

$$\sigma_\ell^\alpha \longrightarrow \sigma_{\ell+1}^\alpha. \tag{1.5}$$

(3) Bond-inversion symmetry P_B:

$$\sigma_\ell^\alpha \longrightarrow \sigma_{L+1-\ell}^\alpha. \tag{1.6}$$

(4) Site-inversion symmetry P_S:

$$\sigma_\ell^\alpha \longrightarrow \sigma_{L+2-\ell}^\alpha. \tag{1.7}$$

The local conservation laws of the XXZ chain, and hence the GGE (1.2), share the first two of these symmetries. However, the higher conservation laws can be odd under the inversion symmetries. For example,

$$H^{(2)}(\Delta) \propto \sum_\ell \epsilon_{\alpha\beta\gamma}\sigma_\ell^\beta\sigma_{\ell+2}^\gamma\sigma_{\ell+1}^\alpha[\Delta + (1-\Delta)\delta_{\alpha,z}] \tag{1.8}$$

is parity odd. The same is true for all $H^{(2n)}$. By construction of the GGE, stationary values of local observables will exhibit the first two symmetries, provided that the GGE indeed describes the late-time behavior after the quench. This implies that if we start out in an initial state that breaks the U(1) or translational symmetry, *they must be restored in the course of the unitary time evolution*. The situation is different for $P_{B,S}$: these are not necessarily restored. However, for the initial states that are invariant under at least one of the reflection symmetries, they will be. This can be seen by noting that as $|\Psi_0\rangle$ is even and $H^{(2n)}$ is odd under the symmetry, we have

$$\langle\Psi_0|H^{(2n)}|\Psi_0\rangle = 0. \tag{1.9}$$

The constraints (1.3) are then fulfilled by setting all Lagrange multipliers λ_{2n} to zero, as can be checked by taking the traces in a basis of simultaneous eigenstates of the Hamiltonian and parity. In other words, the GGE only contains the parity-even conservation laws $H^{(2n+1)}$ in this case, which implies the restoration of the reflection symmetries in the stationary state. All initial states studied below by means of numerical tensor-product methods are of this kind.

II. GENERALIZED GIBBS EXPECTATION VALUES BY THE QUANTUM TRANSFER-MATRIX METHOD

In a recent paper, Fagotti and Essler [8] developed an approach for calculating expectation values of local operators in generalized Gibbs ensembles describing the stationary states for quenches from matrix-product states. Here, we summarize some key results. The density matrix (1.2) can be viewed as describing a thermal (Gibbs) ensemble for an integrable Hamiltonian with long-range interactions. For a given set of Lagrange multipliers $\{\lambda_j\}$, it is then straightforward [8] to generalize the quantum transfer-matrix approach [36] for calculating thermal expectation values to (1.2) (some remarks regarding the structure of the largest eigenvalue of the quantum transfer matrix in our cases are given in Appendix A). In particular, we may use the explicit expressions for short-distance correlators given in Ref. [37], which involve three functions $\varphi(\mu)$, $\omega(\mu_1,\mu_2)$, and $\omega'(\mu_1,\mu_2)$ that encode the necessary information on the density matrix. Examples are

$$\begin{aligned}\langle\sigma_1^z\sigma_2^z\rangle &= \mathrm{cth}(\eta)\omega + \frac{\omega_x'}{\eta},\\ \langle\sigma_1^x\sigma_2^x\rangle &= -\frac{\omega}{2\sinh(\eta)} - \frac{\cosh(\eta)\omega_x'}{2\eta},\end{aligned} \tag{2.1}$$

where $\omega = \omega(0,0)$, $\omega_x' = \partial_x\omega'(x,y)|_{x,y=0}$. Determining the Lagrange multipliers by solving the system (1.3) is a difficult problem [24]. In Ref. [8], a method was introduced that avoids having to calculate them explicitly by working with the generating function

$$\Omega_{\Psi_0}(\lambda) = -i\sum_{k=1}\left(\frac{\eta}{\sinh\eta}\right)^k \frac{\lambda^{k-1}}{(k-1)!}\frac{\langle\Psi_0|H^{(k)}|\Psi_0\rangle}{L}. \tag{2.2}$$

Given $\Omega_{\Psi_0}(\lambda)$, the largest eigenvalue of the quantum transfer matrix, and concomitantly the generalized Gibbs ensemble, is obtained by solving the system of nonlinear integral equations

$$\begin{aligned}\ln\mathfrak{b}(x) - \ln\bar{\mathfrak{b}}(x) + h &= [(k_+ + k) * \ln(1+\mathfrak{b})](x) - [(k_- + k) * \ln(1+\bar{\mathfrak{b}})](x),\\ g_\mu^+(x) &= -d(x-\mu) + \left[k * \frac{g_\mu^+}{1+\mathfrak{b}^{-1}}\right](x) - \left[k_- * \frac{g_\mu^-}{1+\bar{\mathfrak{b}}^{-1}}\right](x),\\ g_\mu^-(x) &= -d(x-\mu) + \left[k * \frac{g_\mu^-}{1+\bar{\mathfrak{b}}^{-1}}\right](x) - \left[k_+ * \frac{g_\mu^+}{1+\mathfrak{b}^{-1}}\right](x),\end{aligned}$$

$$4k(\mu)+\frac{4i}{\eta}\Omega_{\Psi_0}(-2\mu/\eta)=-\int_{-\frac{\pi}{2}}^{\frac{\pi}{2}}\frac{dx}{\pi}d(x)\left(\frac{g_\mu^+(x)}{1+\mathfrak{b}^{-1}(x)}+\frac{g_\mu^-(x)}{1+\bar{\mathfrak{b}}^{-1}(x)}\right),$$
$$4m^z=\int_{-\frac{\pi}{2}}^{\frac{\pi}{2}}\frac{dx}{\pi}\left(\frac{g_0^+(x)}{1+\mathfrak{b}^{-1}(x)}-\frac{g_0^-(x)}{1+\bar{\mathfrak{b}}^{-1}(x)}\right), \tag{2.3}$$

where m^z is the magnetization per site in the initial state, and

$$[f_1*f_2](x)=\int_{-\frac{\pi}{2}}^{\frac{\pi}{2}}\frac{dy}{\pi}f_1(x-y)f_2(y),$$
$$d(x)=\sum_{n=-\infty}^{\infty}\frac{e^{2inx}}{\cosh(\eta n)},\quad k(x)=\sum_{n=-\infty}^{\infty}\frac{e^{2inx}}{e^{2\eta|n|}+1},$$
$$k_\pm(x)=k(x\pm i[\eta-\epsilon]). \tag{2.4}$$

Here, ϵ is a positive infinitesimal. The first three equations of (2.3) have the same form as for the equilibrium problem at finite temperature [37], while the last two equations are different and encode the quench setup and the associated constraints on the expectation values of the higher integrals of motion (1.3). In general, the system (2.3) has to be solved numerically by iteration, and some details on how to do this are presented in Sec. II D. The structure of (2.3) is such that the second and third equations can be straightforwardly inverted (as they are linear) in order to express $g_\mu^\pm$ as functions of $\mathfrak{b}$ and $\bar{\mathfrak{b}}$. The first equation of (2.3) is nonlinear, but nonetheless can be used to express $\bar{\mathfrak{b}}$ in terms of $\mathfrak{b}$. The last equation, which is more conveniently analyzed in Fourier space, can finally be inverted to obtain the remaining unknown $\mathfrak{b}$. The three functions $\varphi(\mu)$, $\omega(\mu_1,\mu_2)$, and $\omega'(\mu_1,\mu_2)$ that enter the expressions for the spin correlation functions are

$$\varphi(\mu)=\int_{-\frac{\pi}{2}}^{\frac{\pi}{2}}\frac{dx}{2\pi}\left(\frac{g_{-i\mu}^-(x)}{1+\bar{\mathfrak{b}}^{-1}(x)}-\frac{g_{-i\mu}^+(x)}{1+\mathfrak{b}^{-1}(x)}\right),$$
$$\omega(\mu_1,\mu_2)=-4k(i\mu_1-i\mu_2)+\tilde{K}_{2\eta}(i\mu_1-i\mu_2)$$
$$-\left[d*\left(\frac{g_{-i\mu_1}^+(x)}{1+\mathfrak{b}^{-1}(x)}+\frac{g_{-i\mu_1}^-(x)}{1+\bar{\mathfrak{b}}^{-1}(x)}\right)\right](-i\mu_2),$$
$$\omega'(\mu_1,\mu_2)=-4\eta\ell(i\mu_1-i\mu_2)+\eta\tilde{K}_{2(\mu_1-\mu_2)}(i\eta)$$
$$-\left[d*\left(\frac{g_{-i\mu_1}'^+}{1+\mathfrak{b}^{-1}}+\frac{g_{-i\mu_1}'^-}{1+\bar{\mathfrak{b}}^{-1}}\right)\right](-i\mu_2)$$
$$-\eta\left[c_-*\frac{g_{-i\mu_1}^+}{1+\mathfrak{b}^{-1}}\right](-i\mu_2)$$
$$-\eta\left[c_+*\frac{g_{-i\mu_1}^-}{1+\bar{\mathfrak{b}}^{-1}}\right](-i\mu_2), \tag{2.5}$$

where

$$\tilde{K}_\eta(x)=\frac{\sinh\eta}{\cosh\eta-\cos(2x)},\quad c_\pm(x)=\pm\sum_{n=-\infty}^{\infty}\frac{e^{\pm\eta n+2inx}}{2\cosh^2(\eta n)},$$
$$\ell(x)=\sum_{n=-\infty}^{\infty}\frac{\mathrm{sgn}(n)e^{2inx}}{4\cosh^2(\eta n)},\quad \ell_\pm(x)=\ell(x\pm i[\eta-\epsilon]), \tag{2.6}$$

and the auxiliary functions $g_\mu'^\pm(x)$ are solutions to the integral equations

$$g_\mu'^+(x)=-\eta c_+(x-\mu)+\eta\left[\ell*\frac{g_\mu^+}{1+\mathfrak{b}^{-1}}\right](x)$$
$$-\eta\left[\ell_-*\frac{g_\mu^-}{1+\bar{\mathfrak{b}}^{-1}}\right](x)+\left[\kappa*\frac{g_\mu'^+}{1+\mathfrak{b}^{-1}}\right](x)$$
$$-\left[\kappa_-*\frac{g_\mu'^-}{1+\bar{\mathfrak{b}}^{-1}}\right](x),$$
$$g_\mu'^-(x)=-\eta c_-(x-\mu)+\eta\left[\ell*\frac{g_\mu^-}{1+\bar{\mathfrak{b}}^{-1}}\right](x)$$
$$-\eta\left[\ell_+*\frac{g_\mu^+}{1+\mathfrak{b}^{-1}}\right](x)+\left[\kappa*\frac{g_\mu'^-}{1+\bar{\mathfrak{b}}^{-1}}\right](x)$$
$$-\left[\kappa_+*\frac{g_\mu'^+}{1+\mathfrak{b}^{-1}}\right](x). \tag{2.7}$$

The method proposed in Ref. [8] for computing spin-spin correlations functions then consists of three main steps:

(1) Calculate the generating function Ω_{Ψ_0}. While this is difficult in general, it was pointed out in Ref. [8] that it can be done efficiently for initial states that are of matrix-product form.

(2) Solve the system (2.3) of nonlinear integral equations for the auxiliary functions $\mathfrak{b}(x)$ and $\bar{\mathfrak{b}}(x)$.

(3) Use the auxiliary functions to determine the functions $\varphi(\mu)$, $\omega(\mu_1,\mu_2)$, and $\omega'(\mu_1,\mu_2)$ and in turn the spin-spin correlation functions.

In the next section, we provide the details of how to calculate Ω_{Ψ_0} for translationally invariant initial states of matrix-product form. The generalization to certain initial states that break translational invariance, e.g., states with Néel order, is considered in Sec. II B. In Sec. II D, we present an efficient numerical algorithm for solving our system of nonlinear integral equations.

Readers not interested in details pertaining to the computation of the generating function (2.2) and the numerical solution of the system of nonlinear integral equations (2.3) may proceed directly to Sec. III.

A. Generating function for translationally invariant matrix-product initial states

Our starting point is the following representation of the generating function derived in Ref. [8]:

$$\Omega_{\Psi_0}(\lambda)=\lim_{L\to\infty}\frac{1}{L}\frac{\partial}{\partial x}\Big|_{x=\lambda}\mathrm{Tr}\langle\Psi_0|V_L(x,\lambda)\dots V_1(x,\lambda)|\Psi_0\rangle, \tag{2.8}$$

where $V_j(x,\lambda)$ are 4×4 matrices with entries $[V_j(x,\lambda)]^{ab}_{cd}$ that are operators acting on the two-dimensional quantum space on site j:

$$[V_j(x,\lambda)]^{ab}_{cd} = [L(x;\sigma_j)]^{ab}[M(\lambda;\sigma_j)]^{cd}. \tag{2.9}$$

Here, L is the L operator of the XXZ model [32] and M is the corresponding matrix associated with the inverse transfer matrix, i.e.,

$$\begin{aligned} L(\lambda;\sigma) &= \frac{1+\tau^z\sigma^z}{2} - i\frac{\sin\left(\frac{\eta\lambda}{2}\right)}{\sinh\left(\eta - i\frac{\eta\lambda}{2}\right)}\frac{1-\tau^z\sigma^z}{2} \\ &\quad + \frac{\sinh(\eta)}{\sinh\left(\eta - i\frac{\eta\lambda}{2}\right)}(\tau^+\sigma^- + \tau^-\sigma^+), \\ M(\lambda;\sigma) &= \frac{1+\mu^z\sigma^z}{2} + i\frac{\sin\left(\frac{\eta\lambda}{2}\right)}{\sinh\left(\eta + i\frac{\eta\lambda}{2}\right)}\frac{1-\mu^z\sigma^z}{2} \\ &\quad + \frac{\sinh(\eta)}{\sinh\left(\eta + i\frac{\eta\lambda}{2}\right)}(\mu^+\sigma^+ + \mu^-\sigma^-), \end{aligned} \tag{2.10}$$

where the Pauli matrices τ^α and μ^α act on distinct auxiliary spaces, which we denote by $\mathcal{T}$ and $\mathcal{M}$, respectively, while σ^α act on the "quantum space" at a given site of the lattice. The trace in (2.8) is over the tensor product $\mathcal{T}\otimes\mathcal{M}\sim\mathbb{C}^4$ of auxiliary spaces, i.e., $\mathrm{Tr}(M) = \sum_{a,b} M^{aa}_{bb}$. A pictorial representation of transfer matrices underlying the construction of the generating function is shown in Fig. 1.

Denoting the two possible spin states at site j (corresponding to spin up and spin down in the z direction, respectively) by $|\pm\rangle_j$, we can construct a basis of the Hilbert space $\mathcal{H}$ of our

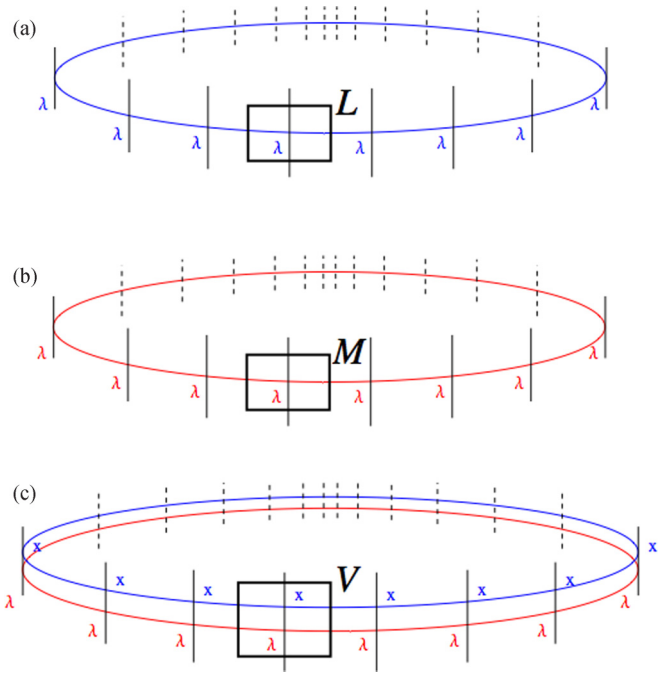

FIG. 1. (Color online) Pictorial representation of the transfer matrices underlying the construction of the generating function $\Omega_{\Psi_0}(\lambda)$. The "two-layer" transfer matrix shown in panel (c) is formed by multiplying the transfer matrices made from the L operators $L(\lambda;\sigma)$ and $M(\lambda;\sigma)$ shown in panels (a) and (b).

L-site lattice by $\{|s_1 s_2 \dots s_L\rangle = \otimes_{j=1}^L |s_j\rangle\,,\ s_\ell = \pm\}$. The most general translationally invariant matrix-product state then can be expressed as

$$\begin{aligned} |\Psi_0\rangle &= \sum_{s_1=\pm}\dots\sum_{s_L=\pm}\mathrm{Tr}_{\mathcal{A}}\left[A^{(s_1)}A^{(s_2)}\dots A^{(s_L)}\right]|s_1\dots s_L\rangle \\ &\equiv \mathrm{Tr}_{\mathcal{A}}[|\hat{\Psi}_{\mathcal{A}}\rangle], \end{aligned} \tag{2.11}$$

where $A^{(\pm)}$ are matrices acting on some auxiliary space $\mathcal{A}$, which we take to be isomorphic to $\mathbb{C}^m$ for some integer m. The normalization condition $\langle\Psi_0|\Psi_0\rangle = 1$ implies that

$$\|[A^{(+)}]^*\otimes A^{(+)} + [A^{(-)}]^*\otimes A^{(-)}\|_{\mathrm{op}} = 1, \tag{2.12}$$

where $\|\dots\|_{\mathrm{op}}$ is the operator norm, i.e., the absolute value of the maximal eigenvalue, which we assume to be nondegenerate. It is customary to restrict the form of the matrix-product state by replacing the condition (2.12) with the stronger requirement

$$A^{(+)}[A^{(+)}]^\dagger + A^{(-)}[A^{(-)}]^\dagger = \mathrm{I}, \tag{2.13}$$

and we adopt this convention in the following. In order to calculate $\Omega_{\Psi_0}(\lambda)$, we require

$$\begin{aligned} &\mathrm{Tr}\langle\Psi_0|V_L(x,\lambda)\dots V_1(x,\lambda)|\Psi_0\rangle \\ &\quad = \mathrm{Tr}_{\mathcal{T}\otimes\mathcal{M}\otimes\bar{\mathcal{A}}\otimes\mathcal{A}}\langle\hat{\Psi}_{\bar{\mathcal{A}}}|V_L(x,\lambda)\dots V_1(x,\lambda)|\hat{\Psi}_{\mathcal{A}}\rangle. \end{aligned} \tag{2.14}$$

As a consequence of translational invariance of (2.11) we have

$$\langle\hat{\Psi}_{\bar{\mathcal{A}}}|V_L(x,\lambda)\dots V_1(x,\lambda)|\hat{\Psi}_{\mathcal{A}}\rangle = [U(x,\lambda)]^L, \tag{2.15}$$

where

$$\begin{aligned} &U(x,\lambda) \\ &= \sum_{s=\pm}\langle s|\left[\sum_{\alpha,\beta=\pm} e_{\alpha\beta}A^{(\alpha)}\otimes(A^{(\beta)})^*\otimes L(x;\sigma)\otimes M(\lambda;\sigma)\right]|s\rangle. \end{aligned} \tag{2.16}$$

Here, $A^{(\pm)}$ act on $\mathcal{A}$, $(A^{(\pm)})^*$ on $\bar{\mathcal{A}}$, and we defined

$$e_{++} = \frac{\mathrm{I}+\sigma^z}{2},\quad e_{+-} = \sigma^+,\quad e_{-+} = \sigma^-,\quad e_{--} = \frac{\mathrm{I}-\sigma^z}{2}. \tag{2.17}$$

By construction, the matrix $U(x,x)$ has an eigenvalue equal to 1. The corresponding right eigenvector $|1;R\rangle$ is independent of x, η, and $A^{(\pm)}$ and can be determined explicitly. If the matrices $A^{(\pm)}$ satisfy (2.13), it has the form

$$\begin{aligned} |1;R\rangle &= \frac{|\uparrow\rangle_{\mathcal{T}}\otimes|\uparrow\rangle_{\mathcal{M}} + |\downarrow\rangle_{\mathcal{T}}\otimes|\downarrow\rangle_{\mathcal{M}}}{\sqrt{2}} \\ &\quad\otimes\left(\sum_{j=1}^m |a_j\rangle_{\mathcal{A}}\otimes|\bar{a}_j\rangle_{\bar{\mathcal{A}}}\right), \end{aligned} \tag{2.18}$$

where the vectors $\{|a_1\rangle,\dots,|a_m\rangle\}$ form an orthonormal basis of $\mathcal{A}$ and $|\bar{a}_j\rangle = |a_j\rangle^*$. In contrast, the left eigenvector of $U(x,x)$ corresponding to the eigenvalue 1 depends in a nontrivial way on x, η, and the initial state. In order to proceed, we assume

that the eigenvalue 1 of $U(x,x)$ is nondegenerate, and that there exists an eigenvalue $u(x,\lambda)$ of $U(x,\lambda)$ that smoothly approaches 1 in the limit $\lambda \to x$. The generating function is then simply equal to

$$\Omega(\lambda) = \frac{\partial}{\partial x}\bigg|_{x=\lambda} u(x,\lambda). \tag{2.19}$$

In practice, the eigenvalue $u(x,\lambda)$ can be calculated in closed form only for very simple initial states. To deal with more general cases, the following representation of the generating function turns out to be very useful:

$$\Omega(\lambda) = \frac{\mathrm{Tr}[\mathrm{adj}[U(\lambda,\lambda)-\mathrm{I}]\partial_x|_{x=\lambda}U(x,\lambda)]}{\mathrm{Tr}[\mathrm{adj}[U(\lambda,\lambda)-\mathrm{I}]]}. \tag{2.20}$$

Here, adj$[M]$ denotes the adjugate, i.e., the transpose of the matrix of cofactors of the matrix M. The representation (2.20) can be established as follows. Since $u(x,\lambda)$ is eigenvalue of $U(x,\lambda)$, we have

$$\det|u(x,\lambda)\mathrm{I} - U(x,\lambda)| = 0, \quad \forall\, x,\lambda. \tag{2.21}$$

The derivative with respect to x is related to the adjugate by Jacobi's formula

$$\partial_x \det|u(x,\lambda)\mathrm{I} - U(x,\lambda)| = \mathrm{Tr}[\mathrm{adj}[u(x,\lambda)\mathrm{I} - U(x,\lambda)]\partial_x[u(x,\lambda)\mathrm{I} - U(x,\lambda)]]. \tag{2.22}$$

By virtue of (2.21), the derivative of the determinant vanishes, so that in the limit $\lambda \to x$ we arrive at

$$0 = \partial_x \mathrm{Tr}[\mathrm{adj}[\mathrm{I} - U(\lambda,\lambda)][u(x,\lambda)\mathrm{I} - U(x,\lambda)]]_{\lambda=x}. \tag{2.23}$$

Combining (2.23) with (2.19), we obtain (2.20).

1. *Explicit expressions for* $\Omega(\lambda)$

In order to determine our generating function from (2.20), we require the two quantities $U(\lambda,\lambda)$ and $\partial_x|_{x=\lambda}U(x,\lambda)$. It is convenient to employ (2.10) in order to rewrite $U(x,\lambda)$ in the form

$$U(x,\lambda) = \frac{1}{e^{\frac{i\eta(\lambda-x)}{2}}\sinh\left(\eta - \frac{i\eta x}{2}\right)\sinh\left(\eta + \frac{i\eta\lambda}{2}\right)}(\mathbb{I},\ e^{-i\eta x/2}\mathbb{I},\ e^{-i\eta x}\mathbb{I})\bar{V}\begin{pmatrix}\mathbb{I}\\ e^{i\eta\lambda/2}\mathbb{I}\\ e^{i\eta\lambda}\mathbb{I}\end{pmatrix}, \tag{2.24}$$

where $\bar{V}$ is a $(12m^2)\times(12m^2)$ matrix *independent of* x *and* λ, and the identities $\mathbb{I}$ are $4m^2 \times 4m^2$ matrices. The two matrices we need in order to calculate the generating function can be expressed as

$$U(\lambda,\lambda) = \frac{2}{\cosh(2\eta)-\cos(\eta\lambda)}(\mathbb{I},\ e^{-i\eta\lambda/2}\mathbb{I},\ e^{-i\eta\lambda}\mathbb{I})\bar{V}\begin{pmatrix}\mathbb{I}\\ e^{i\eta\lambda/2}\mathbb{I}\\ e^{i\eta\lambda}\mathbb{I}\end{pmatrix},$$

$$\partial_x\big|_{x=\lambda}U(x,\lambda) = \frac{i\eta}{1-e^{-2\eta}e^{i\eta\lambda}}U(\lambda,\lambda) - \frac{i\eta}{\cosh(2\eta)-\cos(\eta\lambda)}(0,\ e^{-i\eta\lambda/2}\mathbb{I},\ 2e^{-i\eta\lambda}\mathbb{I})\bar{V}\begin{pmatrix}\mathbb{I}\\ e^{i\eta\lambda/2}\mathbb{I}\\ e^{i\eta\lambda}\mathbb{I}\end{pmatrix}. \tag{2.25}$$

Instead of working with $U(\lambda,\lambda)$ and $\partial_x|_{x=\lambda}U(x,\lambda)$, it is convenient to consider the matrix-valued functions

$$P(\lambda) = e^{i\eta\lambda}[\cosh(2\eta)-\cos(\eta\lambda)][U(\lambda,\lambda)-\mathbb{I}],$$
$$Q(\lambda) = (e^{i\eta\lambda}-e^{-2\eta}e^{2i\eta\lambda})[\cosh(2\eta)-\cos(\eta\lambda)]\partial_x|_{x=\lambda}U(x,\lambda). \tag{2.26}$$

The generating function is related to these functions by

$$\Omega_{\Psi_0}(\lambda) = \frac{1}{(e^{i\eta\lambda}-e^{-2\eta}e^{2i\eta\lambda})[\cosh(2\eta)-\cos(\eta\lambda)]} \times \frac{\mathrm{Tr}\{\mathrm{adj}[P(\lambda)]\ Q(\lambda)\}}{\mathrm{Tr}\{\mathrm{adj}[P(\lambda)]\}}. \tag{2.27}$$

It follows from (2.24) that $P(\lambda)$ is a polynomial (with matrix-valued coefficients) of degree four in the variable $e^{i\frac{\eta\lambda}{2}}$, and its adjugate is a polynomial of degree $4(4m^2-1)$. Hence, the latter is fully determined by evaluating it at $16m^2-3$ different values of λ, which we choose as

$$\lambda_j = \frac{4\pi j}{\eta(16m^2-3)}, \quad j = 0,1,\ldots,16m^2-4. \tag{2.28}$$

The adjugate matrix then takes the form

$$\mathrm{adj}[P(\lambda)] = \frac{1}{16m^2-3}\sum_{n,\ell=0}^{16m^2-4}\mathrm{adj}\,[P(\lambda_\ell)]\ e^{i\frac{n\eta(\lambda-\lambda_\ell)}{2}}, \tag{2.29}$$

which allows us to obtain $\mathrm{adj}[U(\lambda,\lambda)-\mathbb{I}]/\mathrm{Tr}[\mathrm{adj}[U(\lambda,\lambda)-\mathbb{I}]]$ with a numerical effort that scales as m^8. Similarly, the function $Q(\lambda)$ is a fifth-degree polynomial in $e^{i\frac{\eta\lambda}{2}}$, and hence can be expressed as

$$Q(\lambda) = \frac{1}{6}\sum_{j,n=0}^{5}Q(\kappa_j)\,e^{i\frac{n\eta(\lambda-\kappa_j)}{2}}, \quad \kappa_j = \frac{2\pi j}{3\eta}. \tag{2.30}$$

Given an initial matrix-product state of the form (2.11), we numerically compute the matrices adj $[P(\lambda_\ell)]$ and $Q(\kappa_j)$ either exactly or to very high precision, and then use (2.29) and (2.30) to obtain the functions adj $[P(\lambda)]$ and $Q(\lambda)$. In this way, we can extract the value of the finite number of free parameters of the representation (2.27) for the generating functions. We stress that the functional form of $\Omega_{\Psi_0}(\lambda)$ is fixed by the structure of the matrix-product state, and potential inaccuracies of the computation are therefore practically independent of λ.

2. Numerical computation of the generating function

The method discussed in the previous section is most appropriate for exact matrix-product states. In the following, we will be interested in situations where the initial state is only *approximately* of matrix-product form. An example would be the ground state of the Heisenberg chain for large anisotropy Δ. In such cases, we resort to a faster, fully numerical computation of the generating function by means of the representation (2.20). Employing a singular value decomposition we have

$$U(\lambda,\lambda)-\mathbb{I}=\mathcal{U}(\lambda)\mathcal{D}(\lambda)\mathcal{V}^{\dagger}(\lambda), \tag{2.31}$$

where $\mathcal{U}(\lambda)$ and $\mathcal{V}(\lambda)$ are unitary matrices and $\mathcal{D}(\lambda)$ is a positive-semidefinite diagonal matrix. As $U(\lambda,\lambda)$ has a non-degenerate eigenvalue equal to 1, the adjugate of $U(\lambda,\lambda)-\mathbb{I}$ is of rank one, so that the singular value decomposition becomes

$$\mathrm{adj}[U(\lambda,\lambda)-\mathbb{I}]=\det{}_{+}|\mathcal{D}(\lambda)|\vec{v}_R(\lambda)\vec{v}_L^{\dagger}(\lambda). \tag{2.32}$$

Here, $\det_+$ denotes the pseudodeterminant, i.e., the product of the nonzero eigenvalues, and $\vec{v}_{R/L}(x)$ are the normalized right and left singular vectors corresponding to the unique nonzero singular value. The generating function takes the form

$$\Omega_{\Psi_0}(\lambda)=\frac{\vec{v}_L^{\dagger}(\lambda)[\partial_x|_{x=\lambda}U(x,\lambda)]\vec{v}_R(\lambda)}{\vec{v}_L^{\dagger}(\lambda)\vec{v}_R(\lambda)} \tag{2.33}$$

and, for a given λ, can be straightforwardly computed with a computational effort that scales as m^6 (using the detailed structure of the matrices, it is in principle possible to significantly reduce the numerical complexity [38]). Compared to (2.27), the representation (2.33) is numerically better behaved. On the other hand, the representation (2.27) has the advantage of providing the exact form of the generating function. In order to solve the system (2.3) of nonlinear integral equations, we will require the values of $\Omega(\lambda)$ in a complex domain. For the initial states we consider this domain is the strip $|\mathrm{Im}(\lambda)|<1$. As $\Omega(\lambda)$ is a $\frac{2\pi}{\eta}$-periodic function, it can be conveniently expanded in a Fourier series

$$\Omega_{\Psi_0}(\lambda)=i\eta\sum_n \omega_n e^{i\eta n\lambda}. \tag{2.34}$$

In practice, we retain only a finite number of Fourier coefficients, which we determine using (2.33).

B. Initial states that break translational invariance

In the previous section, we showed how to determine the generating function for translationally invariant matrix-product initial states. Here, we consider generalizations to certain simple classes of states that break translational invariance.

1. States with Néel order

In the ground state of XXZ chain at $\Delta>1$, translational invariance is broken spontaneously, and in order to describe interaction quenches $H^{(1)}(\Delta_0)\to H^{(1)}(\Delta)$ in the antiferromagnetic phase, we therefore need to generalize the analysis of Sec. II A. The spontaneous breaking of translational symmetry to translations by two sites can be addressed by employing a simple unitary transformation

$$\begin{aligned}H^{(1)}(\Delta)\longrightarrow&\left[\prod_\ell\sigma^x_{2\ell}\right]H^{(1)}(\Delta)\left[\prod_\ell\sigma^x_{2\ell}\right]\\&=\frac{1}{4}\sum_{\ell=1}^{L}\sigma^x_\ell\sigma^x_{\ell+1}-\sigma^y_\ell\sigma^y_{\ell+1}-\Delta\big(\sigma^z_\ell\sigma^z_{\ell+1}+1\big).\end{aligned} \tag{2.35}$$

In the limit of large Δ, the ground states of the transformed Hamiltonian are ferromagnetic with all spins up or down, respectively. Spontaneous symmetry breaking selects one of them, but crucially the resulting ground state is translationally invariant, and can be approximated by a matrix-product state of the form (2.11). Reversing the unitary transformation, we are led to consider matrix-product states of the form

$$\begin{aligned}|\mathrm{GS};\Delta_0\rangle&=\left[\prod_\ell\sigma^x_{2\ell}\right]\sum_{s_1,\dots,s_L}\mathrm{Tr}_{\mathcal{A}}\big[A^{(s_1)}\dots A^{(s_L)}\big]|s_1\dots s_L\rangle\\&\equiv\left[\prod_\ell\sigma^x_{2\ell}\right]|\Psi_0\rangle.\end{aligned} \tag{2.36}$$

The corresponding generating function is then

$$\begin{aligned}\Omega_{|\mathrm{GS},\Delta_0\rangle}(\lambda)=\lim_{L\to\infty}\frac{1}{L}\frac{\partial}{\partial x}\bigg|_{x=\lambda}&\mathrm{Tr}\langle\mathrm{GS};\Delta_0|\\&\times V_L(x,\lambda)\dots V_1(x,\lambda)|\mathrm{GS};\Delta_0\rangle,\end{aligned} \tag{2.37}$$

where $V_n(x,\lambda)$ are given in (2.9). The evaluation of (2.37) can be reduced to the same calculation as in the translationally invariant case by noting that

$$\begin{aligned}&\mathrm{Tr}\langle\mathrm{GS};\Delta_0|V_L(x,\lambda)\dots V_1(x,\lambda)|\mathrm{GS};\Delta_0\rangle\\&=\mathrm{Tr}\langle\Psi_0|\left[\prod_\ell\sigma^x_{2\ell}\right]V_L(x,\lambda)\dots V_1(x,\lambda)\left[\prod_\ell\sigma^x_{2\ell}\right]|\Psi_0\rangle\\&=\mathrm{Tr}\langle\Psi_0|\widetilde{V}_L(x,\lambda)\dots\widetilde{V}_1(x,\lambda)|\Psi_0\rangle,\end{aligned} \tag{2.38}$$

where

$$(\widetilde{V}_j(x,\lambda))^{ab}_{cd}=[\tau^x L(x;\sigma_j)]^{ab}[\mu^x M(\lambda;\sigma_j)]^{cd}. \tag{2.39}$$

In order to derive (2.38), we have used the property

$$[L(x;\sigma)M(\lambda;\sigma),\sigma^x\tau^x\mu^x]=0, \tag{2.40}$$

which follows from the definitions (2.10) of L and M. We note that the simple reduction (2.38) does not generalize straightforwardly to states with Néel order in a direction tilted away from the z axis.

2. Matrix-product states obtained via DMRG

Matrix-product states obtained by density-matrix renormalization group (DMRG) methods on open chains lack translation invariance. Such computations typically result in

states of the form

$$|\mathrm{MPS}\rangle = \left[\prod_\ell \sigma^x_{2\ell}\right] \sum_{s_1,\ldots,s_L} \mathrm{Tr}_{\mathcal{A}}\left[\tilde{A}_1^{(s_1)}\tilde{A}_2^{(s_2)}\ldots\tilde{A}_L^{(s_L)}\right]|s_1\ldots s_L\rangle, \tag{2.41}$$

$$\tilde{A}_j^{(s_j)} = P_j A^{(s_j)} P_{j+1}^{-1}, \quad |2j-L| \ll L, \tag{2.42}$$

where, in the bulk of the system, the matrices P_j are often diagonal with elements ± 1. In the following, we will assume this property to hold. The "gauge transformation" (2.42) obscures translational invariance, and in order to apply our method for calculating the generating function we would like to make the state manifestly invariant. By virtue of (2.42), the state (2.41) has the same bulk properties as

$$\left[\prod_\ell \sigma^x_{2\ell}\right] \sum_{s_1,\ldots,s_L} \mathrm{Tr}_{\mathcal{A}}[A^{(s_1)}A^{(s_2)}\ldots A^{(s_L)}]|s_1\ldots s_L\rangle, \tag{2.43}$$

which can be dealt with by the method outlined in Sec. II B 1. This leaves us with the problem of how to obtain the matrices $A^{(\pm)}$ for a state of the form (2.41) and (2.42). This can be done by picking a site $\bar{j}$ that is sufficiently far away from the boundaries. The matrix

$$B^{(s)} = \tilde{A}^{(s)}_{\bar{j}} P_{\bar{j}} P_{\bar{j}+1} \tag{2.44}$$

is related to $A^{(s)}$ by the similarity transformation $B^{(s)} = P_{\bar{j}} A^{(s)} P_{\bar{j}}$ (note that $P_{\bar{j}}^2 = \mathbb{I}$), and can be used to replace $A^{(s)}$ in (2.43). Since both $P_{\bar{j}-1}P_{\bar{j}}$ and $P_{\bar{j}}P_{\bar{j}+1}$ are simple diagonal matrices with elements ± 1, i.e., at most $2m$ unknowns, the (approximate) $m \times m$ matrix equation [cf. (2.42)]

$$\tilde{A}^{(s)}_{\bar{j}-1} \approx P_{\bar{j}-1}P_{\bar{j}}\tilde{A}^{(s)}_{\bar{j}}P_{\bar{j}}P_{\bar{j}+1} \tag{2.45}$$

can generally be used to extract both $P_{\bar{j}}P_{\bar{j}+1}$ and $P_{\bar{j}-1}P_{\bar{j}}$. Knowing $P_{\bar{j}}P_{\bar{j}+1}$, (2.44) gives $B^{(s)}$ in turn, and therefore we obtained a translation-invariant representation of the state.

C. Closed-form expressions for the generating function of some simple initial states

We have calculated $\Omega_{\Psi_0}(\lambda)$ analytically for a variety of initial states, which are invariant under translations by n sites. The case $n > 1$ is dealt with by a straightforward generalization of Eq. (2.15), in which the matrix $U(x,\lambda)$ is associated with a block of n adjacent spins. Among the states we considered are as follows:

(1) Néel state in the z direction (in spin space) $|\uparrow\downarrow\uparrow\downarrow\ldots\rangle$:

$$\Omega_{|\uparrow\downarrow\uparrow\downarrow\ldots\rangle}(\lambda) = \frac{i\eta}{2}\frac{\sinh(2\eta)}{\cosh(2\eta)+1-2\cos(\eta\lambda)}. \tag{2.46}$$

(2) Néel state in the x direction $|{\rightarrow}{\leftarrow}{\rightarrow}{\leftarrow}\ldots\rangle$:

$$\Omega_{|\rightarrow\leftarrow\rightarrow\leftarrow\ldots\rangle} = \frac{i\eta}{2}\frac{\sinh(\eta)}{2\cosh(\eta)-1-\cos(\eta\lambda)}. \tag{2.47}$$

(3) Ferromagnet along the x direction $|{\rightarrow}{\rightarrow}\ldots\rangle$:

$$\Omega_{|\rightarrow\rightarrow\ldots\rangle} = \frac{i\eta}{2}\frac{\sinh(\eta)}{2\cosh(\eta)+1+\cos(\eta\lambda)}. \tag{2.48}$$

(4) Majumdar-Ghosh dimer product state $|\mathrm{MG}\rangle = \prod_{j=1}^{L/2} \frac{|\uparrow\rangle_{2j-1}\otimes|\downarrow\rangle_{2j}-|\downarrow\rangle_{2j-1}\otimes|\uparrow\rangle_{2j}}{2}$:

$$\Omega_{|\mathrm{MG}\rangle} = \frac{i\eta\sinh(\eta)}{2}\frac{4\cos(\eta\lambda)[\sinh^2(\eta)-\cosh(\eta)]+\cosh(\eta)+2\cosh(2\eta)+3\cosh(3\eta)-2}{4[\cosh(2\eta)-\cos(\eta\lambda)]^2}. \tag{2.49}$$

We note that $|\mathrm{MG}\rangle$ is one of two ground states of the Hamiltonian

$$H_{\mathrm{MG}} = J_1\sum_j \mathbf{S}_j\cdot\mathbf{S}_{j+1} + \frac{J_1}{2}\sum_j \mathbf{S}_j\cdot\mathbf{S}_{j+2}. \tag{2.50}$$

(5) Ferromagnetic domain state $|\mathrm{FD}\rangle = |\ldots\underbrace{\downarrow\ldots\downarrow}_{s}\underbrace{\uparrow\ldots\uparrow}_{s}\underbrace{\downarrow\ldots\downarrow}_{s}\underbrace{\uparrow\ldots\uparrow}_{s}\ldots\rangle$:

$$\Omega_{|\mathrm{FD}\rangle} = \frac{i\eta}{2s}\coth(\eta)\tanh\left[\frac{s}{2}\ln\left(\frac{\cosh(2\eta)-\cos(\eta\lambda)}{1-\cos(\eta\lambda)}\right)\right]. \tag{2.51}$$

(6) Tilted ferromagnet $|\theta;\nearrow\nearrow\ldots\rangle = e^{i\theta\sum_j S^y_j}|\uparrow\uparrow\ldots\rangle$:

$$\Omega_{|\theta;\nearrow\nearrow\ldots\rangle} = \frac{i\eta\ \sinh\eta\sin^2\theta}{[\cos(2\theta)+3]\cos(\eta\lambda)+4\cosh\eta+2\ \sin^2\theta}. \tag{2.52}$$

This state has a magnetization per site in the z direction of $\frac{\cos\theta}{2}$.

(7) Tilted Néel state $|\theta;\nearrow\swarrow\ldots\rangle = e^{i\theta\sum_j S^y_j}|\uparrow\downarrow\ldots\rangle$:

$$\Omega_{|\theta;\nearrow\swarrow\ldots\rangle} = \frac{i\eta\ \sinh\eta\{2\ \sin^2\theta\cos(\eta\lambda)+\cosh\eta[\cos(2\theta)+3]\}}{D(\theta)},$$

$$D(\theta) = -2\sin^2\theta\ \cos(2\eta\lambda)+2\cos(\eta\lambda)\left[-2\ \cosh^2\left(\frac{\eta}{2}\right)\cos(2\theta)+\cosh\eta-3\right]$$
$$+2\cos(2\theta)\cosh\eta-2\cosh\eta+4\cosh(2\eta)+\cos(2\theta)+3. \tag{2.53}$$

TABLE I. Symmetries on the various initial states.

	State	U(1)	m^z	Translations	Site inversion	Bond inversion
1.	$\|\uparrow\downarrow\ldots\rangle$	Yes	0	By 2 sites	Yes	No
2.	$\|\rightarrow\leftarrow\ldots\rangle$	No	0	By 2 sites	Yes	No
3.	$\|\rightarrow\rightarrow\ldots\rangle$	No	0	Yes	Yes	Yes
4.	$\|\mathrm{MG}\rangle$	Yes	0	By 2 sites	No	Yes
5.	$\|\mathrm{FD}\rangle$	Yes	0	No	No	No
6.	$\|\theta;\nearrow\nearrow\ldots\rangle$	No	$\frac{1}{2}\cos\theta$	Yes	Yes	Yes
7.	$\|\theta;\nearrow\swarrow\ldots\rangle$	No	0	By 2 sites	Yes	No

These initial states break some of the continuous or discrete symmetries of the post-quench Hamiltonian discussed in Sec. I A. Table I summarizes their symmetry properties.

D. Numerical solution of the system of nonlinear integral equations

The system (2.3) of nonlinear integral equations generally needs to be solved by iteration. A convenient limit in which this can be done "by hand" is the case of a "small" quench for $m^z = 0$ considered in Ref. [8]. This corresponds to the regime $|\mathfrak{b}|, |\bar{\mathfrak{b}}| \ll 1$ because in the relevant domain $|\mathrm{Im}[x]| < 1$, the generating function $\Omega(x)$ is close to the analogous quantity evaluated in the ground state of the post-quench Hamiltonian (and concomitantly the expectation values of the integrals of motion deviate only slightly from their ground-state values). At the lowest order in the iteration, one finds [8]

$$\mathfrak{b}(x) \approx \bar{\mathfrak{b}}(x) \approx \rho^{(1)}(x) = \frac{\frac{i}{\eta}\Omega_{\Psi_0}\left(-\frac{2x}{\eta}+i\right) + \frac{i}{\eta}\Omega_{\Psi_0}\left(-\frac{2x}{\eta}-i\right) + \frac{\sinh(\eta)}{\cosh(\eta)-\cos(2x)}}{d(x)}, \tag{2.54}$$

where $d(x)$ has been defined above in (2.4). For more general quenches, the system (2.3) needs to be solved numerically, and we now provide some details about how this can be done. We find it convenient to work in the Fourier space, where (2.3) turns into a nonlinear system of equations for the Fourier coefficients of $\mathfrak{b}$ and $\bar{\mathfrak{b}}$. Since the latter are generally smooth functions, a good approximation can be achieved by retaining only a finite number $\sim n_{\max}$ of Fourier coefficients (the error being exponentially small in $n_{\max}$). Although formally there is no problem in writing the equations in different ways, in practice the objects defined in each step of the process must have Fourier coefficients that can be safely neglected at high frequency. This is an important point to which we return later.

We start by introducing some useful notations. We denote by $[f]$ the Toeplitz matrix with elements

$$[f]_n^\ell = \int_{-\frac{\pi}{2}}^{\frac{\pi}{2}} \frac{dx}{\pi} e^{-2i(n-\ell)x} f(x). \tag{2.55}$$

By extension, $[f]^0$ is the vector of Fourier coefficients

$$[f]_n^0 = \int_{-\frac{\pi}{2}}^{\frac{\pi}{2}} \frac{dx}{\pi} e^{-2inx} f(x). \tag{2.56}$$

In these notations, we have, e.g.,

$$[d]_n^\ell = \frac{1}{\cosh[\eta(n-\ell)]}. \tag{2.57}$$

We further introduce the following matrices constructed from the Fourier coefficients of $k(x)$, $k_\pm(x)$, and $d(x)$ [cf. (2.4)], respectively,

$$K_n^\ell = \frac{\delta_n^\ell}{e^{2\eta|n|}+1}, \quad (K_\pm)_n^\ell = \frac{\delta_n^\ell e^{\mp 2\eta n}}{e^{2\eta|n|}+1}, \qquad D_n^\ell = \frac{\delta_n^\ell}{\cosh(\eta n)}, \quad (\mathbb{I}_{\mathrm{H}})_{n\ell} = \delta_n^{-\ell}. \tag{2.58}$$

We note that in these expressions round brackets have no special meaning. We further define two matrices $G_\pm$ with elements

$$(G_\pm)_n^\alpha = \chi^{\mp 1} \iint_{[-\pi/2,\pi/2]^2} \frac{dx\, d\mu}{\pi^2} e^{-2inx-2i\alpha\mu} g_\mu^\pm(x), \tag{2.59}$$

where χ is a real, positive parameter that equals 1 if $m^z = 0$. Finally, we parametrize the auxiliary functions $\mathfrak{b}(x)$ and $\bar{\mathfrak{b}}(x)$ as follows [8]:

$$\frac{1}{1+\mathfrak{b}^{-1}(x)} = \chi\rho(x)e^{\zeta(x)/2}, \qquad \frac{1}{1+\bar{\mathfrak{b}}^{-1}(x)} = \chi^{-1}\rho(x)e^{-\zeta(x)/2}. \tag{2.60}$$

The system (2.3) of nonlinear integral equations can then be recast in the compact form

$$\chi = \frac{1}{2m^z-1}\sum_\alpha (G_+)_0^\alpha \equiv -\frac{2m^z+1}{\sum_\alpha (G_-)_0^\alpha}, \tag{2.61}$$

$$[\zeta]_n^0 = 2e^{-\eta|n|}\sinh(\eta n)[\ln(1-\chi^{\mathrm{sgn}(n)}e^{\mathrm{sgn}(n)\zeta/2}\rho)]_n^0, \tag{2.62}$$

$$[\rho]^0 = 2[1/d]\,\mathbb{I}_{\mathrm{H}}\Lambda_-(\Lambda_-+\Lambda_+)^{-1}\Lambda_+\mathbb{I}_{\mathrm{H}}\,[d]\,[\rho^{(1)}]^0, \tag{2.63}$$

$$G_\pm = -[e^{\mp\zeta/2}](\Lambda_\pm^T)^{-1}\mathbb{I}_{\mathrm{H}}D, \tag{2.64}$$

where $\Lambda_\pm$ are the transposes of the matrices

$$\Lambda_\pm^T = (\chi^{\pm 1}[e^{\pm\zeta/2}] - K[\rho])(\chi^{\pm 1}[e^{\pm\zeta/2}] - (K+K_\mp)[\rho])^{-1} \times (\chi^{\mp 1}[e^{\mp\zeta/2}] - (K+K_\pm)[\rho]) + K_\pm[\rho]. \tag{2.65}$$

An approximate solution of (2.61) can now be obtained as follows:

(1) The system (2.61) is finitized by constraining the indices of the infinite-dimensional matrices and vectors to be contained in the set $n \in [-n_{\max}, n_{\max}]$.

(2) The resulting nonlinear equations are solved by iteration. In each step, only a single function is updated, in particular, the second (third) equation of (2.61) is used to iterate ζ (ρ). Each equation is solved separately by iteration in order to reach an intermediate accuracy goal, which is updated only after all unknowns have met the same criterion.

Some comments are in order. In all quenches we considered, the density $\rho^{(1)}(x)$ given in (2.54) is a smooth function. Hence, the elements of the vector $[\rho^{(1)}]^0$ "decay exponentially from the center," i.e., only the elements $[\rho^{(1)}]^0_n$ with $n \approx 0$ are significantly different from zero. The same holds true for the vector $\mathbb{I}_{\mathrm{H}}[d][\rho^{(1)}]^0$. In order to be able to neglect the high-frequency contribution and approximate $[\rho^{(1)}]^0$ by a vector with a finite number of elements, the matrix $\Lambda_-(\Lambda_- + \Lambda_+)^{-1}\Lambda_+$ (cf. the third equation) should not have large elements that connect high-frequency components with low-frequency ones. This is indeed what we observe in all cases considered. This justifies our finitization procedure for all quantities appearing in (2.63). Similarly, we find that finitizing the matrix $G_\pm$ in (2.64) induces only exponentially small (in $n_{\max}$) errors in (2.61). Equation (2.62) is more problematic. Although in all cases we considered we succeeded in obtaining solutions such that the function $\zeta(x)$ is smooth, in the course of the computation the function inside the logarithm can develop zeros, with catastrophic consequences. This can be controlled using under-relaxation and/or preconditioning the equation (the appropriate transformations are quench dependent).

In order to obtain results for short-distance correlation functions, we require expressions for the auxiliary functions $g'^{\pm}_{\mu}(x)$ defined in (2.7). In Fourier space, Eqs. (2.7) take the form

$$\begin{aligned} G'_\pm &= [e^{\mp\zeta/2}][\chi^{\mp 1}[e^{\mp\zeta/2}] \\ &\quad - K[\rho] - K_\mp[\rho](\chi[e^{\pm\zeta/2}] - K[\rho])^{-1}K_\pm[\rho]]^{-1} \\ &\quad \times [M_\pm - K_\mp[\rho](\chi^{\pm 1}[e^{\pm\zeta/2}] - K[\rho])^{-1}M_\mp], \end{aligned} \tag{2.66}$$

where

$$\begin{aligned} (G'_\pm)^\alpha_n &= \chi^{\mp 1}\int_{-\frac{\pi}{2}}^{\frac{\pi}{2}}\frac{dx}{\pi}\int_{-\frac{\pi}{2}}^{\frac{\pi}{2}}\frac{d\mu}{\pi}e^{-2inx-2i\alpha\mu}g'^{\pm}_{\mu}(x), \\ (M_\pm)^\alpha_n &= \frac{\eta[\mathrm{sgn}(n)e^{\eta|n|} \mp e^{\pm\eta n}]}{2\cosh^2(\eta n)}\delta^{-\alpha}_n \\ &\quad + \eta\chi^{\mp 1}\frac{\mathrm{sgn}(n)e^{-\eta|n|}}{2\cosh(\eta n)}(G_\pm)^\alpha_n. \end{aligned} \tag{2.67}$$

1. *Simplifications for parity-symmetric states*

Parity-symmetric initial states have the property

$$\Omega(-x) = \Omega(x), \tag{2.68}$$

which leads to a number of simplifications. From (2.54), it follows that

$$[\rho^{(1)}]^0_n = \left([\rho^{(1)}]^0_n\right)^* = [\rho^{(1)}]^0_{-n}, \tag{2.69}$$

which in turn permits a solution of (2.61) in terms of real $[\rho]_n$, $[\zeta]_n$, and χ. If the magnetization m^z vanishes, additional simplifications occur:

(i) The parameter χ is equal to 1.

(ii) $[\rho]^0_n = [\rho]^0_{-n} = ([\rho]^0_n)^*$, i.e., $\mathbb{I}_{\mathrm{H}}[f(\rho)]\mathbb{I}_{\mathrm{H}} = [f(\rho)]$.

(iii) $[\zeta]^0_n = -[\zeta]^0_{-n} = ([\zeta]^0_n)^*$, i.e., $\mathbb{I}_{\mathrm{H}}[f(\zeta)]\mathbb{I}_{\mathrm{H}} = [f(-\zeta)]$.

(iv) $\Lambda_- = \mathbb{I}_{\mathrm{H}}\Lambda_+\mathbb{I}_{\mathrm{H}}$, $M_- = -\mathbb{I}_{\mathrm{H}}M_+\mathbb{I}_{\mathrm{H}}$, $G_- = \mathbb{I}_{\mathrm{H}}G_+\mathbb{I}_{\mathrm{H}}$, and $G'_- = -\mathbb{I}_{\mathrm{H}}G'_+\mathbb{I}_{\mathrm{H}}$.

In particular, we no longer require the equation for χ and we can write the second equation of (2.61) as follows:

$$[\zeta]^0_n = \frac{2\tanh(\eta n)}{1+\kappa\tanh(\eta|n|)}\left[\ln\left(e^{(\kappa-1)\frac{\zeta}{2}} - \rho e^{\frac{\kappa\zeta}{2}}\right)\right]^0_{|n|}, \tag{2.70}$$

where κ is an auxiliary parameter aimed at stabilizing the iterative process and/or enhancing the convergence rate (notice that the solution does not depend on κ).

2. *Results for some initial states*

In this section, we present results of the numerical solution of our system (2.3) of nonlinear integral equations for several quenches with $m_z = 0$. We focus on the auxiliary functions $\rho(x)$ and $\zeta(x)$ defined in (2.60). Let us define

$$\begin{aligned} \mathcal{E}(x) &= \frac{\sinh\eta}{2}\sum_{j=0}\lambda_{j+1}\left(\frac{\sinh\eta}{2}\frac{d}{dx}\right)^j d(x) \\ &\equiv [k * \ln(1+\mathfrak{b})](x) - [k_- * \ln(1+\bar{\mathfrak{b}})](x) - \ln\mathfrak{b}(x), \end{aligned} \tag{2.71}$$

where the second equality is a by-product of the integral equations [8]. We note that if the Lagrange multipliers fulfill certain conditions (cf. Ref. [39])which in particular should lead to $\mathcal{E}(x)$ being positive, $\mathcal{E}(x)$ can be interpreted as a *dressed energy* associated with the "Hamiltonian" characterizing the GGE density matrix (1.2):

$$H_{\mathrm{GGE}} = \sum_{\ell=1}\lambda_\ell H^{(\ell)}. \tag{2.72}$$

Having possible interpretations of this kind in mind, we quote the analogous result for the Gibbs ensemble at temperature T as a point of reference [36]:

$$\mathcal{E}_{\mathrm{Gibbs}}(x) = \frac{1}{T}\frac{\sinh\eta}{2}d(x). \tag{2.73}$$

By construction, this is proportional to the usual zero-temperature dressed energy of the Heisenberg XXZ chain [40]. Following, we compare $\rho(x)$ and $\zeta(x)$ to the corresponding functions that solve the equilibrium *finite-temperature* nonlinear integral equations [37]. The latter can be obtained by replacing the fourth equation of (2.3) by (2.71), with $\mathcal{E}_{\mathrm{Gibbs}}(x)$ of Eq. (2.73) taking the place of $\mathcal{E}(x)$; the temperature T is fixed via the requirement that the average energy in the Gibbs ensemble associated with the post-quench Hamiltonian is equal to the energy in the initial state after the quench

$$\langle\Psi_0|H^{(1)}|\Psi_0\rangle = \frac{\mathrm{Tr}[e^{-H^{(1)}/T}H^{(1)}]}{\mathrm{Tr}[e^{-H^{(1)}/T}]}. \tag{2.74}$$

Figures 2–7 show results obtained from a numerical solution of the system (2.3).

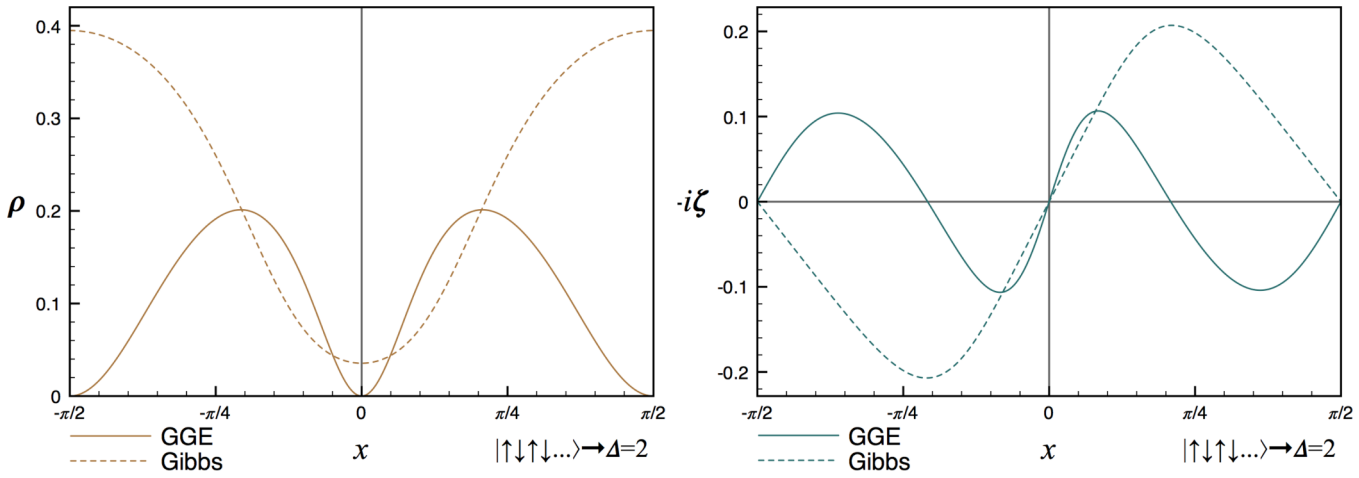

FIG. 2. (Color online) Interaction quench from $\Delta_0 = \infty$. The auxiliary function $\rho(x)$ vanishes at $x = 0, \frac{\pi}{2}$. The dashed lines show ρ (left) and ζ (right) at a temperature T corresponding to the expectation value of energy in the initial state. The shape of the auxiliary functions does not change significantly if Δ_0 is taken to be large but finite.

In all quenches we considered, $\mathcal{E}(x)$ is very different from $\mathcal{E}_{\rm Gibbs}(x)$. This agrees with general expectations based on Ref. [39]. A peculiar feature arising in many quenches (see, e.g., Figs. 2–6) is the presence of zeros in $\rho(x)$, which are associated with logarithmic singularities of $\mathcal{E}(x)$. Ultimately, such singularities are a consequence of the long-range nature of $H_{\rm GGE}$ for these quenches, i.e., the magnitudes of the Lagrange multipliers λ_ℓ decay very slowly with ℓ. Very similar singular behavior has previously been reported in $H_{\rm GGE}$ after quenches in models that have free fermionic spectra. In these cases, the singular behavior was traced back to the fact that the initial state is an eigenstate of (generally nonlocal) conservation laws [12,41]. Such a relation holds true for the XXZ chain as well: the appropriate (nonlocal) charges are given by

$$Q(k) = \frac{1}{\sinh\eta}\sum_{j=0}\frac{1}{j!}\left[\left(\frac{-2k-i\eta}{\sinh\eta}\right)^j + \left(\frac{-2k+i\eta}{\sinh\eta}\right)^j\right] \times \frac{H^{(j+1)}}{L} + \frac{\sinh\eta}{\cosh\eta-\cos(2k)}$$

$$\equiv \frac{i}{\eta L}\left[\tau'\left(-\frac{2k}{\eta}\right)\tau^{-1}\left(-\frac{2k}{\eta}\right) + \tau'\left(2i-\frac{2k}{\eta}\right)\tau^{-1} \times \left(2i-\frac{2k}{\eta}\right)\right] + \frac{\sinh\eta}{\cosh\eta-\cos(2k)}. \quad (2.75)$$

Here, τ is the transfer matrix of the XXZ model

$$\tau(i+\lambda) = \mathrm{Tr}_{\mathcal{T}}\left[\prod_j L(\lambda;\sigma_j)\right], \quad (2.76)$$

where the L operator $L(\lambda;\sigma_j)$ is defined in (2.10) and $\mathcal{T}$ denotes the auxiliary space (on which the τ^α act). The additive constant and the normalization have been chosen in such a way that

$$\langle\Psi_0|Q(k)|\Psi_0\rangle = \rho^{(1)}(k)d(k), \quad (2.77)$$

where $\rho^{(1)}$ is defined in (2.54). Therefore, the "small-quench limit" of Ref. [8] corresponds to the regime $\langle\Psi_0|Q(k)|\Psi_0\rangle \ll 1$.

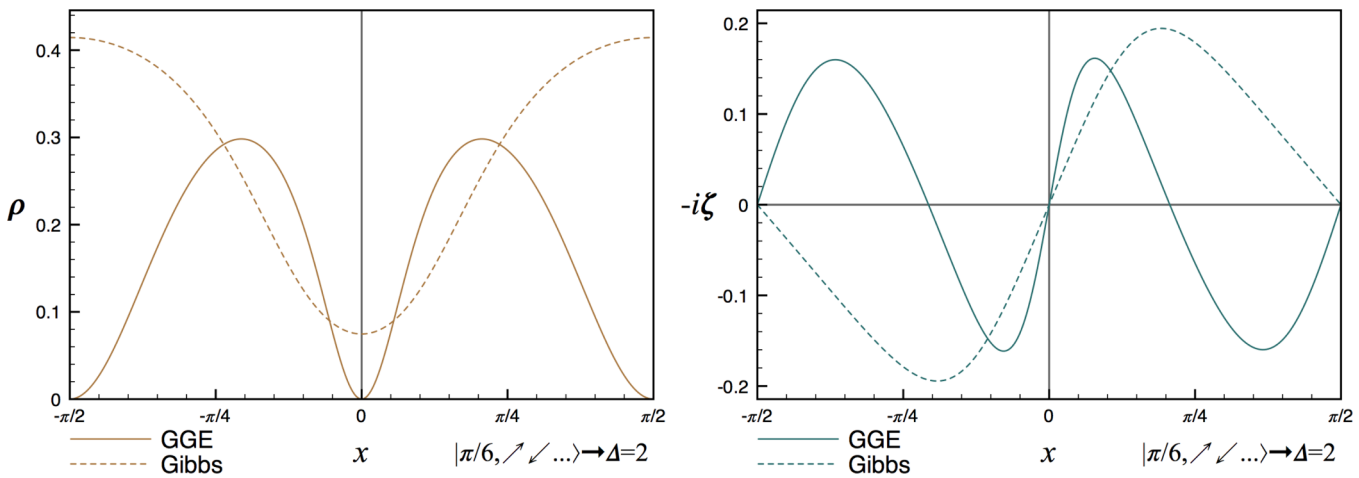

FIG. 3. (Color online) Quench from the tilted Néel state $|\pi/6, \nearrow\swarrow \ldots\rangle$. The auxiliary function $\rho(x)$ vanishes at $x = 0, \frac{\pi}{2}$.

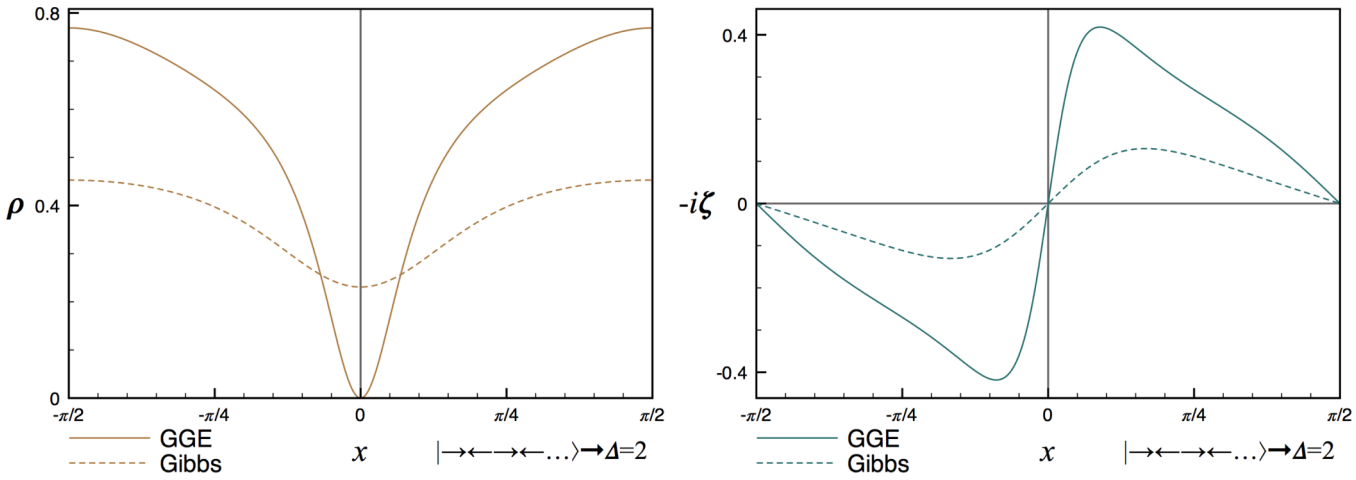

FIG. 4. (Color online) Quench from the Néel state in the x direction $|\rightarrow\leftarrow\rightarrow\leftarrow\ldots\rangle$. The auxiliary function $\rho(x)$ vanishes at $x = 0$.

Using the identity

$$\frac{1}{2}\sum_{j=0}\frac{1}{j!}\left[\left(\frac{-2y-i\eta}{\sinh\eta}\right)^j+\left(\frac{-2y+i\eta}{\sinh\eta}\right)^j\right]\times\left(\frac{\sinh\eta}{2}\frac{d}{dx}\right)^j d(x)=\pi\delta(x-y),\quad x,y\in\left(-\frac{\pi}{2},\frac{\pi}{2}\right) \tag{2.78}$$

one then finds

$$\frac{H_{\rm GGE}}{L}\sim\int_{-\frac{\pi}{2}}^{\frac{\pi}{2}}\frac{dk}{\pi}\mathcal{E}(k)\left(Q(k)-\frac{\sinh\eta}{\cosh\eta-\cos(2k)}\right). \tag{2.79}$$

This is to be interpreted as the density matrices corresponding to the operators on the two sides of the equation yielding identical local properties. If $\mathcal{E}(k)$ diverges at a particular value k_0, the Lagrange multiplier of the conserved charge $Q(k_0)$ is infinite, which implies that only a subspace of the Hilbert space contributes to the generalized Gibbs ensemble.

In the transverse-field Ising chain, the long-time behavior of transverse correlations [11] after a quench of the transverse field is determined precisely by the degrees of freedom that are almost "frozen" by the above mechanism. In particular, transverse correlations decay at late times such as $t^{-3/2}$ rather than the naive expectation $t^{-1/2}$ because the Bogoliubov modes with momenta 0 and π are removed by the aforementioned projection mechanism: the initial state is an eigenstate of the conserved charges $Q_0 = \alpha_0^\dagger\alpha_0$ and $Q_\pi = \alpha_\pi^\dagger\alpha_\pi$. These observations suggest the possibility that in the XXZ case zeros in $\rho(x)$ might affect the late-time behavior of observables in a similar fashion.

III. NUMERICAL RESULTS

In this section, we present extensive numerical studies of the quench dynamics of the XXZ chain with $\Delta > 1$ by means of the time-dependent density matrix renormalization group (tDRMG) [42] and infinite time-evolving block-decimation (iTEBD) [43] algorithms. The latter has the advantage of working directly in infinite systems avoiding both finite-size and revival effects. However, since as well known, the main limitation to the working of both algorithms is the fast growth of the entanglement entropy after a global quantum quench, for any practical purpose the two techniques are equivalent. The tDMRG computations are performed on finite chains of

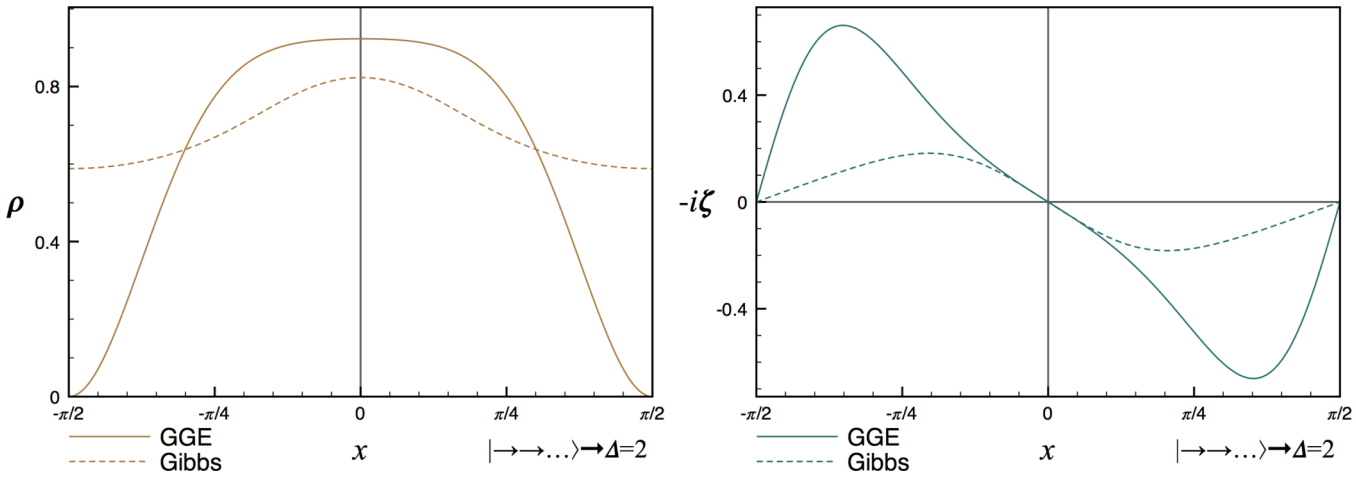

FIG. 5. (Color online) Quench from the ferromagnetic state in the x direction $|\rightarrow\rightarrow\ldots\rangle$. The auxiliary function $\rho(x)$ vanishes at $x = \frac{\pi}{2}$.

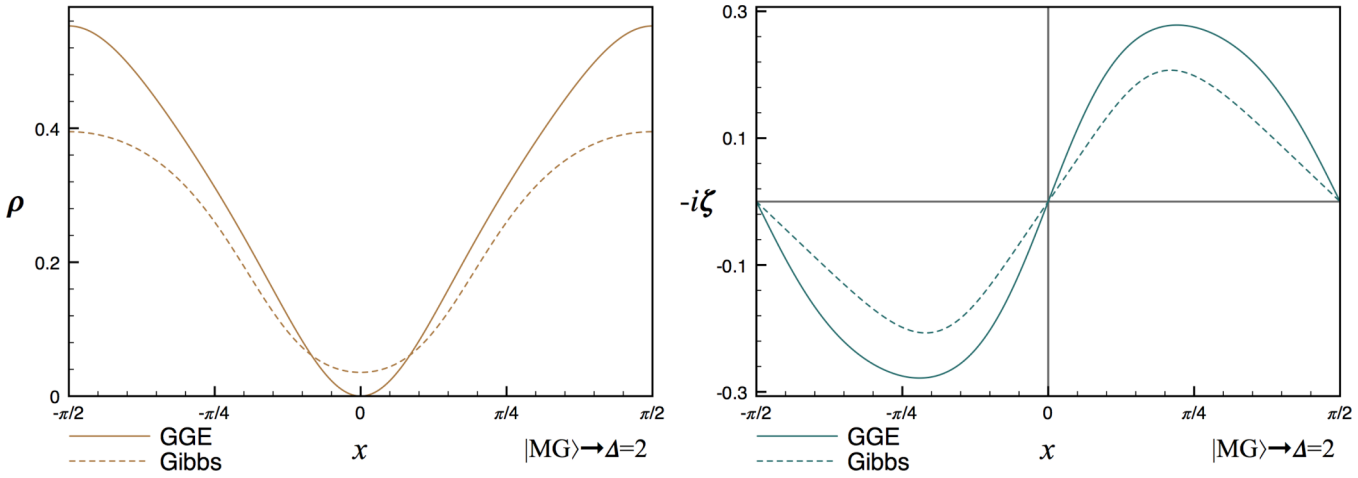

FIG. 6. (Color online) Quench from the ground state of the Majumdar-Ghosh model. The auxiliary function $\rho(x)$ vanishes at $x = 0$.

L spins (L is taken to be even) with open boundary conditions

$$H = J \sum_{j=1}^{L-1} \left(S_j^x S_{j+1}^x + S_j^y S_{j+1}^y + \Delta\, S_j^z S_{j+1}^z \right). \qquad (3.1)$$

In the following, we will set $J = 1$. The late-time behavior of short-range correlators will then be compared with the GGE predictions obtained from the numerical solution of the system of nonlinear integral equations reported in Sec. II. Depending on the initial state, the relevant generating function (2.2) is computed either numerically or analytically.

A. Details of the tDMRG analysis

When necessary, the algorithm initially performs a static subroutine which selects the initial state $|\Psi_0\rangle$ as the ground state of a given Hamiltonian. In the decimation process of this static subroutine, we keep a number of states such that the energy precision is at least of the order of 10^{-12}. Subsequently, we perform the evolution using the time-adapting block-decimation procedure implemented both in tDMRG and iTEBD codes. In the tDMRG code, we always use open boundary conditions. We use the second-order (and in some cases the fourth-order) Suzuki-Trotter decomposition of the evolution operator with time step dt which varies in the range $[5 \times 10^{-3}, 5 \times 10^{-4}]$. We checked the stability of the results with the change of dt in order to be sure that no systematic errors are introduced by time discretization. In the tDMRG code, for each time step, the local evolution operator is applied sequentially on each bond starting form the left boundary of the chain and going to the right border and coming back. We adapt in time the number of states used to describe the reduced Hilbert space retaining at each local step all those eigenvectors of the reduced density matrix corresponding to eigenvalues larger than $\lambda_{\min} \in [10^{-18}, 10^{-20}]$, up to a maximum value $\chi_{\mathrm{MAX}} \in [300, 1000]$ (clearly the effective maximal value used by the algorithm strongly depends on the simulation parameters). For the iTEBD, thanks to the invariance under two-site shift, we need only to apply the local evolution operator twice (on the odd and on the even bounds, see Ref. [43] for details). In this algorithm, the number of states is kept fixed to χ_{MAX} from the beginning of the simulation.

In order to check the GGE predictions, we focus our attention on the following two-point spin-spin correlation

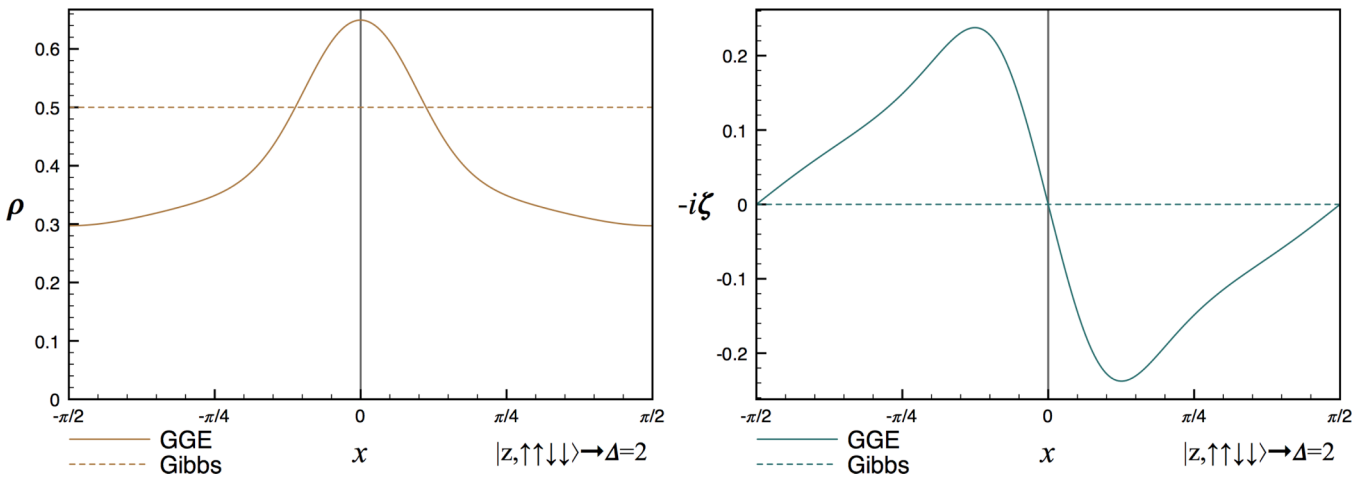

FIG. 7. (Color online) Quench from the $s = 2$ ferromagnetic domain state $|\ldots\uparrow\uparrow\downarrow\downarrow\uparrow\uparrow\downarrow\downarrow\ldots\rangle$. The effective temperature of the Gibbs ensemble is infinite, as one can immediately infer from $\langle H^{(1)} \rangle = 2^{-L} \mathrm{Tr}[H^{(1)}]$.

functions:

$$S^{\alpha}_{j,j+\ell} = \langle \Psi_0(t)|\sigma^{\alpha}_j \sigma^{\alpha}_{j+\ell}|\Psi_0(t)\rangle, \quad \ell = 1,2,3, \quad \alpha = x,y,z. \tag{3.2}$$

Here, $\sigma^{\alpha}_j \equiv 2S^{\alpha}_j$ are Pauli matrices. The iTEBD algorithm operates directly in the thermodynamic limit and hence the choice of j in $S^{\alpha}_{j,j+\ell}$ (i.e., the location of the first spin in the two-point function we are computing) is irrelevant in the sense that any breaking of translational invariance is entirely induced by the initial state and not due to finite-size effects. This is not the case for tDMRG simulations, which are performed in finite systems (of total even length L). Thus, in order to avoid spurious boundary effects for the largest possible time, we measure the correlators in the middle of the chain, i.e.,

$$\begin{aligned} F_{\alpha 1} &\equiv S^{\alpha}_{\frac{L}{2},\frac{L}{2}+1}, \quad F_{\alpha 2} \equiv S^{\alpha}_{\frac{L}{2},\frac{L}{2}+2}, \\ F_{\alpha 3} &\equiv S^{\alpha}_{\frac{L}{2}-1,\frac{L}{2}+2}, \quad \alpha = x,y,z. \end{aligned} \tag{3.3}$$

A list with explicit results for the expected stationary values of (3.3) is presented in Appendix B. Even for correlators in the middle of the chain, boundary effects will start to be felt after a certain time. Such unwanted effects are easily detected, e.g., by checking when the entanglement entropy of the left half stops growing linearly in time. In all the plots reported in the following, only data unaffected by such boundary effects are presented.

After having under control all other sources of systematic errors (i.e., discretization of time and finite sizes), the only limitation of the numerical algorithms is given by the finite number of states kept in the decimation. Indeed, the computational complexity of the time evolution of a quantum system on a classical computer using any algorithm based on matrix-product states (including tDMRG and iTEBD) is essentially set by the growth of the bipartite entanglement. In general for a global quantum quench, the entanglement entropy is expected to grow linearly with time [44]. In Fig. 8, we report the growth of the half-system entanglement entropy with time for some representative initial states and evolving with the XXZ Hamiltonian for $\Delta = 2$: in all cases, we have an asymptotic linear increase, but the slope varies considerably from quench to quench. Consequently, as the entanglement increases, we have to increase exponentially with time the dimension χ of the reduced Hilbert space in order to optimally control the truncation error. In spite of the adaptive choice of χ, the truncation procedure remains the main source of error of the algorithm.

For most of the quenches studied in the following we have used both algorithms and checked that the data are equivalent. However, for the largest times reported, the simulations are numerically demanding and we have chosen one of the two algorithms to avoid costing duplications. In the main text, we will discuss the numerical data without specifying every time the used algorithm which will be reported only in the caption of the figures.

B. Tilted Néel state

We first consider the evolution from a Néel state pointing in an arbitrary direction in the xz plane, i.e., from the initial state

$$|\theta; \nearrow\swarrow \ldots\rangle = e^{i\theta \sum_j S^y_j}|\uparrow\downarrow \ldots\rangle. \tag{3.4}$$

The Néel state in the z direction ($\theta = 0^\circ$) respects the U(1) symmetry of the Hamiltonian and leads to isotropic correlations in the transverse directions, i.e., $S^x_{j,j+k} = S^y_{j,j+k}$. Results for quenches from this state to $H^{(1)}(\Delta = 2)$ and $H^{(1)}(\Delta = 4)$ are presented in Figs. 9 and 10, respectively.

We observe that all correlation functions appear to relax to time-independent values, which are compatible with the predictions of the GGE. The quench originating from the Néel state has been thoroughly analyzed previously, and our results are in perfect agreement with those reported in Ref. [45]. In particular, the oscillatory behavior during

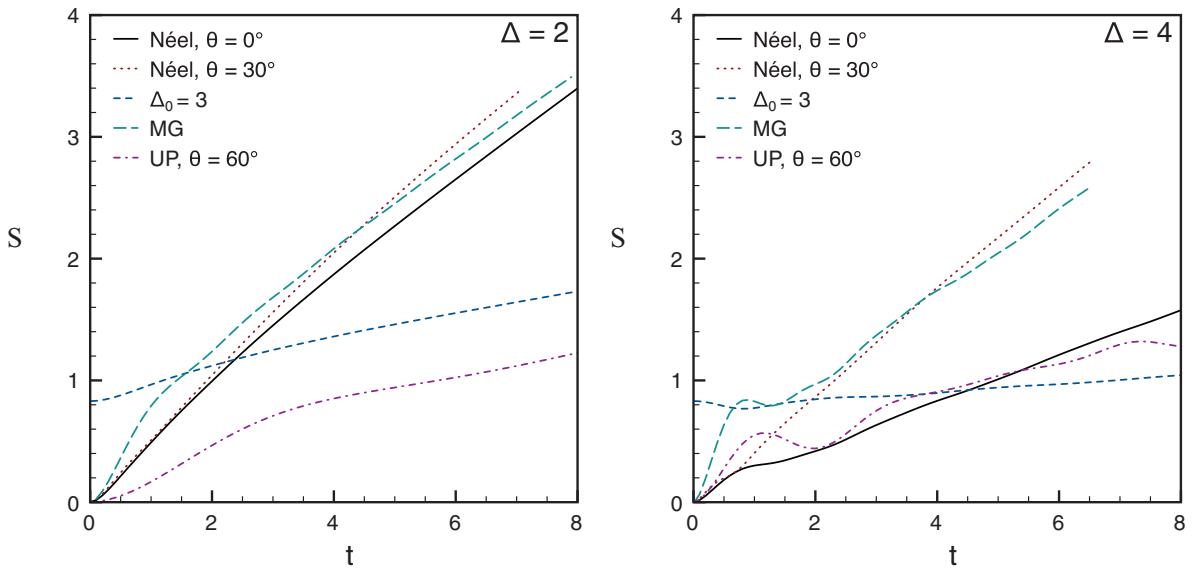

FIG. 8. (Color online) Time evolution of the half-system entanglement entropy for quenches starting from several initial states considered in the text to XXZ chains with $\Delta = 2$ (left) and 4 (right), respectively.

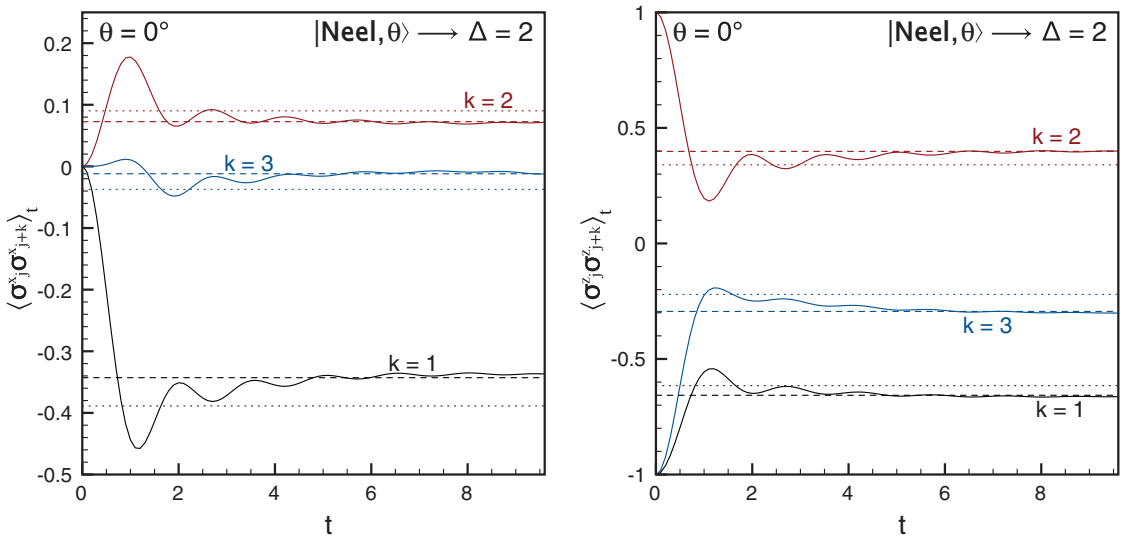

FIG. 9. (Color online) tDMRG results on a chain of $L = 64$ sites for a quench from a Néel state along the z direction (i.e., with $\theta = 0^\circ$) to $\Delta = 2$. Left panel: transverse spin correlations [$S^x_{j,j+k} = S^y_{j,j+k}$ as the initial state respects the U(1) spin-rotational symmetry of $H^{(1)}(\Delta)$]. Right panel: longitudinal correlations. The dashed lines indicate the GGE predictions, which are seen to be approached fairly quickly. The dotted lines are the thermal expectation values (at the finite temperature given by the energy of the initial state) which are well separated from the GGE.

relaxation reflects the presence of multiple frequencies, with the principal frequency proportional to the anisotropy [45] Δ. Hence, the larger the value of Δ, the easier it is to observe the relaxation because the oscillations around the asymptotic value are faster. In the figures, we also report the Gibbs values at temperatures fixed by the initial-state energies. It is evident that, in some cases, these values are well separated from the GGE ones and those are the ideal candidates to distinguish the two ensembles in real experiments.

Next, we consider quenches from Néel states where the order parameter points along an arbitrary direction, a situation which to the best of our knowledge has not been previously considered in the literature. This case presents a very interesting difference compared to the Néel state in the z direction: for any nonzero tilt θ the initial state breaks the rotational symmetry in the xy plane of the XXZ Hamiltonian. This means that transverse correlations in the x and y directions are no longer required to be equal by symmetry, and at short times they are indeed generically quite different. On the other hand, in the GGE the U(1) symmetry is restored. It is therefore important to understand on what time scales the symmetry restoration occurs. In Figs. 11–14, we report results for quenches from tilted Néel states at angles $\theta = 10^\circ$, 20°, and 30°, respectively. In all cases, the transverse correlations are seen to relax in an oscillatory manner to stationary values compatible with restoration of the spin-rotational symmetry around the z axis. As in the $\theta = 0$ case, the oscillations are irregular (indeed even more irregular than before), which

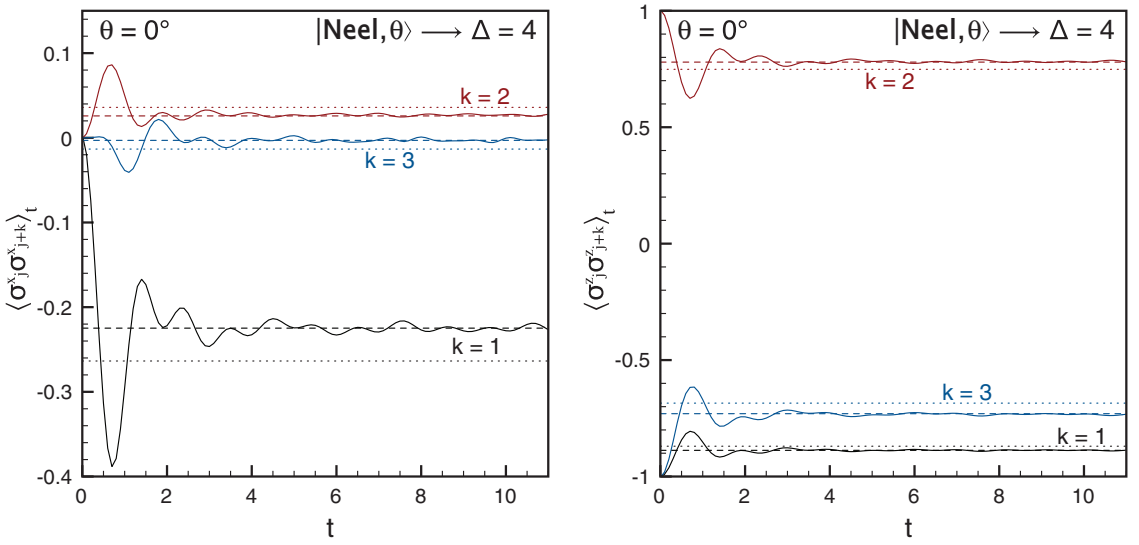

FIG. 10. (Color online) Same as Fig. 9, but with $\Delta = 4$.

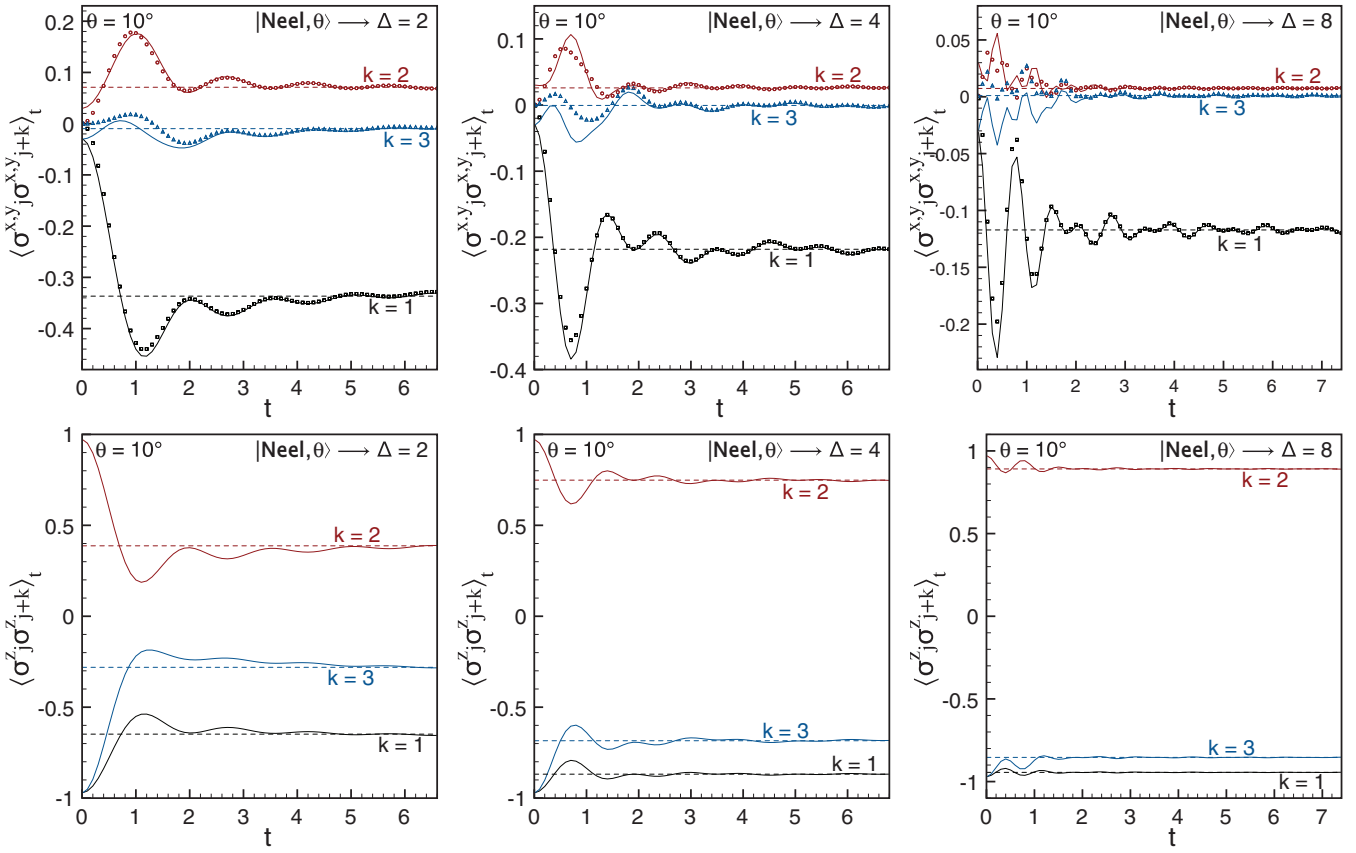

FIG. 11. (Color online) Quench from a Néel state with $\theta = 10^\circ$ to $\Delta = 2,4,8$ (from left to right). Top row: transverse correlations $\langle\sigma^x_j\sigma^x_{j+k}\rangle_t$ (solid lines) and $\langle\sigma^y_j\sigma^y_{j+k}\rangle_t$ (symbols) for distances $k = 1,2,3$. The rotational symmetry in the xy plane is restored at $t \approx 2$. Bottom row: longitudinal correlations for distances $k = 1,2,3$. All correlators approach the GGE predictions (dashed lines) at late times.

indicates the presence of multiple frequencies. The principal frequency again appears to be proportional to the anisotropy Δ. As a result, it is easier to observe the relaxation for large Δ because the oscillations around the asymptotic value are faster. In fact, for $\Delta = 2$, the correlations do not look particularly stationary even at the latest times accessible to us because they oscillate around their asymptotic values with a very large period.

Another interesting issue is the influence of the *strength* of the U(1) symmetry breaking in the initial state: clearly increasing θ leads to a stronger breaking of the symmetry, and the naive expectation would be that this results in a slower relaxation to a stationary regime. Interestingly, this expectation is not entirely borne out by the numerical results: a comparison of Figs. 11–14 indicates that the symmetry is restored (in the sense that $S^x_{j,j+k}$ becomes approximately equal to $S^y_{j,j+k}$) on a time scale that appears to not be strongly θ dependent. From a computational point of view, decreasing the values of θ leads to an increase in the required computational resources because the entanglement entropy grows more quickly (cf. Fig. 8).

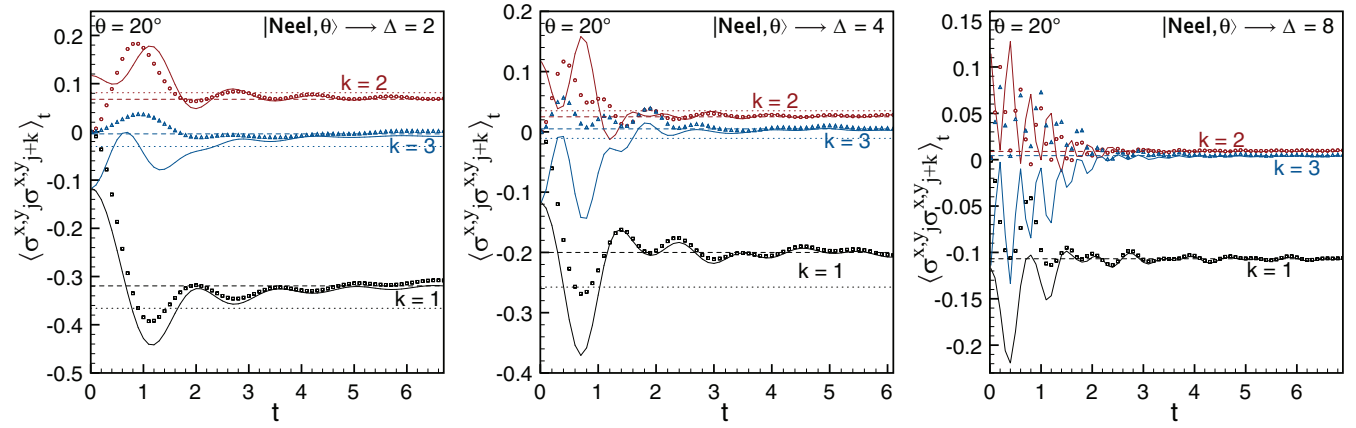

FIG. 12. (Color online) Same as Fig. 11, but with initial state with $\theta = 20^\circ$.

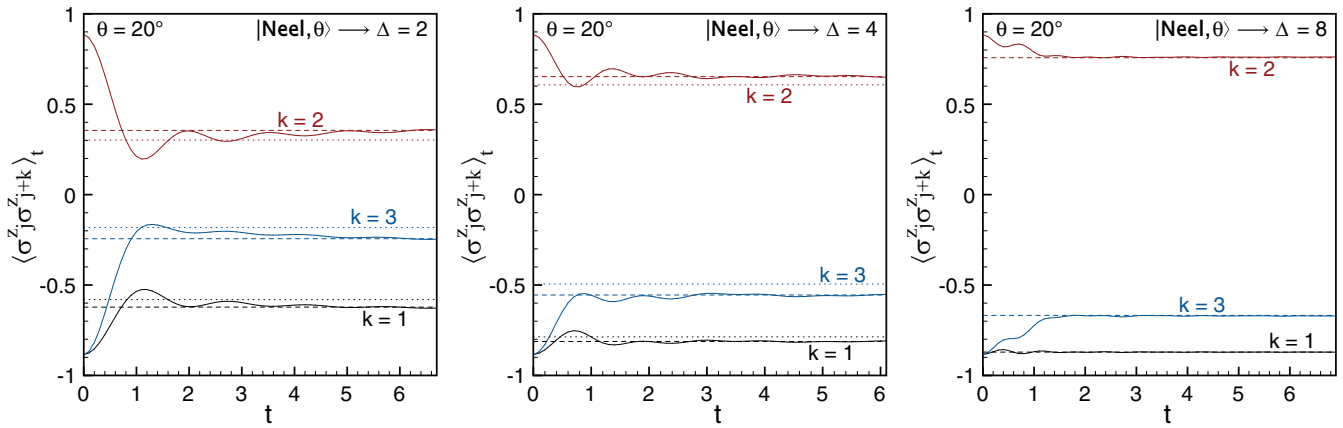

FIG. 13. (Color online) Same as Fig. 11, but with initial state with $\theta = 20^\circ$.

This makes the simulations increasingly difficult for initial states aligned closer to the $\hat{x}$ axis.

C. Majumdar-Ghosh dimer product state

We now turn to time evolution starting in the Majumdar-Ghosh ground state

$$|\mathrm{MG}\rangle = \prod_{j=1}^{L/2} \frac{|\uparrow\rangle_{2j-1} \otimes |\downarrow\rangle_{2j} - |\downarrow\rangle_{2j-1} \otimes |\uparrow\rangle_{2j}}{2}. \quad (3.5)$$

This quench exhibits very interesting physical features, but is also quite demanding numerically (for Δ larger than $\simeq 1.4$) because of the fast growth of the entanglement entropy (cf. Fig. 8, where the entanglement growth is comparable with the Néel state with $\theta = 30^\circ$). The state (3.5) breaks translational invariance, while the GGE is translationally invariant. This implies that translational symmetry should get restored. In order to analyze this symmetry restoration, we compute correlators with even and odd parities using tDRMG, i.e., $\langle \mathrm{MG}(t)|\sigma^\alpha_{L/2}\sigma^\alpha_{L/2+k}|\mathrm{MG}(t)\rangle$ and $\langle \mathrm{MG}(t)|\sigma^\alpha_{L/2-1}\sigma^\alpha_{L/2-1+k}|\mathrm{MG}(t)\rangle$ for $\alpha = x,z$ and $k = 1,3$. We note that it is sufficient to consider transverse correlations in the x direction, as the initial state is U(1) invariant. Furthermore, as $|\mathrm{MG}\rangle$ is invariant under translations by two

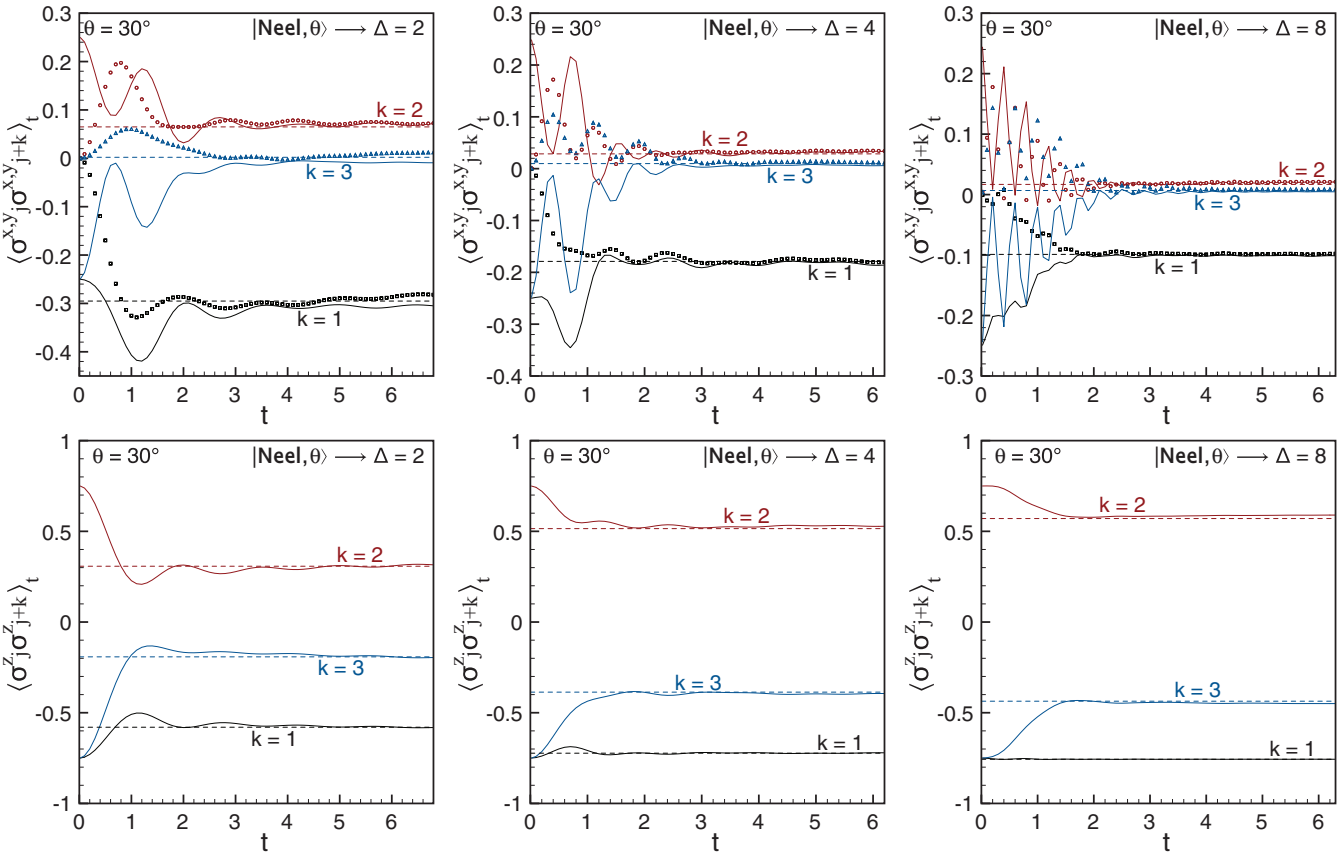

FIG. 14. (Color online) The same as Fig. 11, but with initial state with $\theta = 30^\circ$.

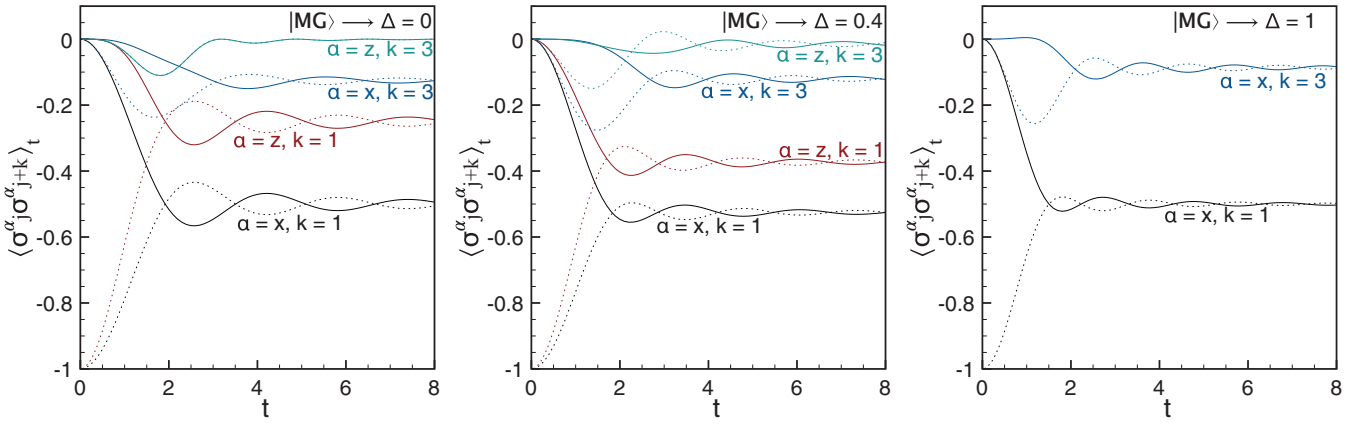

FIG. 15. (Color online) Quench from the Majumdar-Ghosh state to different $\Delta \geqslant 0$. We focus on correlators at distances 1 and 3, as nearest-neighbor correlations are insensitive to translational symmetry breaking and the data approach the GGE values quite rapidly. Solid (dotted) lines correspond to $j = L/2$ and $L/2 - 1$, respectively. For small values of Δ, relaxation to stationary values is observed. For small values of $\Delta > 1$, the observed relaxation is compatible with the predictions of the GGE (dashed lines). For larger values of Δ, relaxation does not occur on the accessible time scales.

sites, next-nearest-neighbor correlators are insensitive to the breaking of translational symmetry.

In Figs 15, 16, and 17, we show the time evolution of transverse and longitudinal correlations at distances 1 and 3 for quenches to the Heisenberg chain with several values of Δ. We include results for $\Delta \leqslant 1$ in order to elucidate the general trend of the Δ dependence. The $\Delta = 0$ case is exactly solvable by free-fermion methods [46], and our numerical results agree perfectly with the analytical results in this case. At late times, all correlations relax in an oscillatory manner to stationary values given by the appropriate GGE. The qualitative behavior of correlation functions is essentially unchanged for anisotropies smaller than $\Delta = 1$, but GGE predictions for the stationary values are not yet available. Increasing Δ further, the time evolution is seen to become less regular, involving several oscillation frequencies. The curves for parity-even and -odd correlators cease to be symmetric around the stationary value and the relaxation is observed to slow down. The results for $\Delta = 1.2, 1.4, 1.6$ are visibly compatible with relaxation to the GGE predictions (dashed lines). For $\Delta = 2, 4, 8$, no relaxation is observed on the accessible time scales. This strongly suggests a relaxation time that grows with increasing Δ. In fact, one can show that in the limit $\Delta \to \infty$, the relaxation time diverges [46].

D. Tilted ferromagnetic state

In this case, the initial state is

$$|\theta; \nearrow\nearrow \ldots\rangle = e^{i\theta \sum_j S^y_j} |\uparrow\uparrow \ldots\rangle. \tag{3.6}$$

The tilted ferromagnetic states are similar to the tilted Néel states in that they generally break the U(1) symmetry of rotations around the z axis of the XXZ Hamiltonian. However, the quench is more complicated than in the Néel case for the following reason. The ferromagnetic state along the z axis ($\theta = 0$) does not break the U(1) symmetry, but in fact is an eigenstate of the XXZ Hamiltonian. As a result, spin-spin correlation functions are time independent in this case. When we approach $\theta = 0^\circ$ from above, the breaking of symmetry becomes unimportant, while at the same time it becomes increasingly difficult to observe relaxational behavior in the accessible time window. Furthermore, a ferromagnetic state in an arbitrary direction is an exact eigenstate of the isotropic ($\Delta = 1$) Hamiltonian. Concomitantly, the relaxation

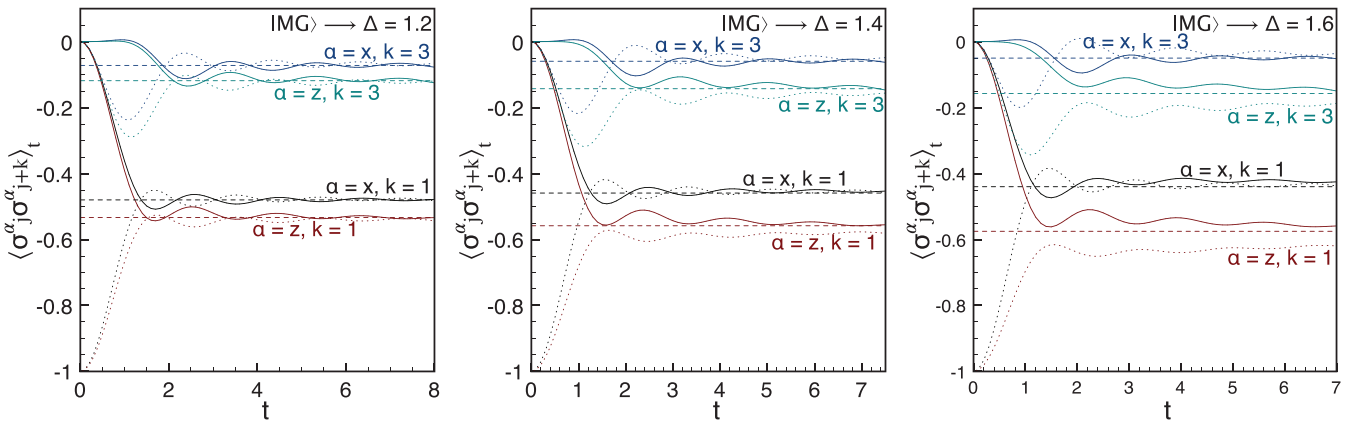

FIG. 16. (Color online) Same as Fig. 15, with $\Delta = 1.2, 1.4, 1.6$.

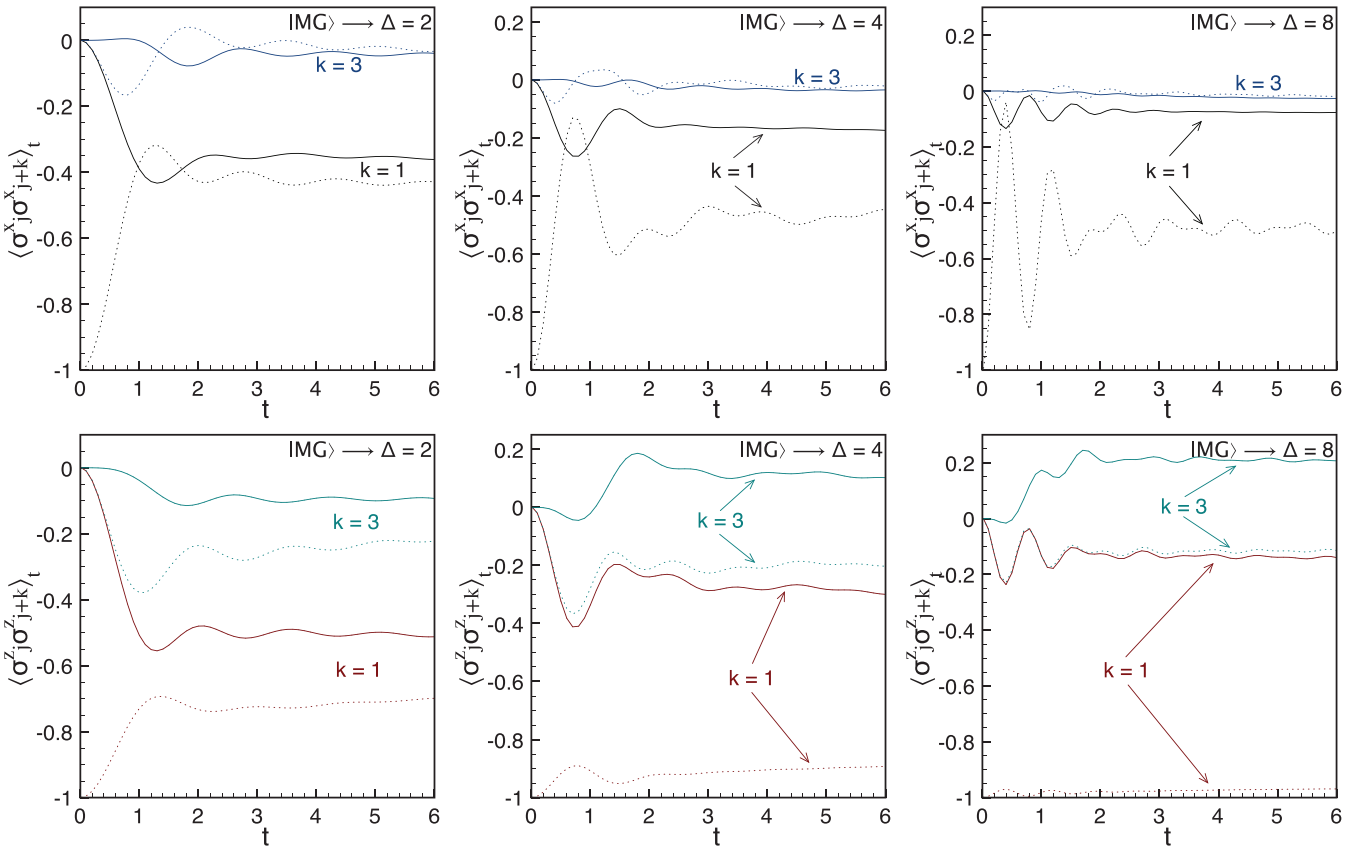

FIG. 17. (Color online) Same as Fig. 15, with $\Delta = 2,4,8$. Transverse and longitudinal correlations are shown separately for the sake of clarity.

time diverges for quenches from general tilted ferromagnetic states when Δ is close to 1. As a result of the aforementioned complications, the relaxation times are always extraordinarily large and even though the growth of the entanglement entropy is considerably slower than for the other initial states we have considered (cf. Fig. 8), which allows us to explore larger time windows, relaxation to the GGE is not observed during the accessible times.

In Figs. 18 and 19, we show iTEBD data for quenches from tilted ferromagnetic states with $\theta = 90^\circ, 60^\circ, 30^\circ$ to an XXZ chain with $\Delta = 4$. The various correlators are seen to exhibit irregular and nonmonotonic oscillations. The symmetry in the xy plane is clearly not restored. The observed oscillatory behavior in the nearest-neighbor correlations occurs around values that are broadly compatible with the GGE prediction. Conversely, correlators at distances 2 and 3 appear to relax, but to values that are quite distant from the GGE predictions. Our interpretation of the data is that in all cases the time scale for relaxation is too large to be accessible by numerical simulations.

In order to lend credence to this interpretation, we have analyzed the single-spin expectation values $\langle \sigma_j^{x,y} \rangle$ for a quench from a ferromagnetic state with $\theta = 30^\circ$ to $\Delta = 8$. The results are shown in Fig. 20. The data are compatible with exponential relaxation to the expected GGE value zero, but with a very large relaxation time. In order to see whether there is any evidence for restoration of spin-rotational symmetry around the z axis, it is useful to plot the differences between transverse correlators $|\langle \sigma_j^x \sigma_{j+k}^x \rangle - \langle \sigma_j^y \sigma_{j+k}^y \rangle|$ for distances $k = 1,2,3$ as functions of time. The data are compatible with a very slow exponential decay to zero, indicating symmetry restoration at very late times. A naive fit of the maxima for the difference at $k = 1$ gives a time scale $\tau \sim 130$, which implies that in order to observe the true asymptotic value with a precision of 0.01, we should roughly run the simulation up to $t \sim 300$, which is clearly beyond our capability. For smaller values of Δ, the relaxation times increase because we are getting closer to the isotropic point $\Delta = 1$, where relaxation is absent. Consequently, an analysis as in Fig. 20 becomes even more difficult, but we are confident that the same qualitative scenario is valid. The upshot is as follows: We believe that quenches starting from tilted ferromagnetic states are characterized by very large relaxation times. This prevents us from checking the GGE predictions.

E. Interaction quenches

The final class of initial states we have considered are ground states of the Heisenberg XXZ chain, i.e., *interaction quenches*, where we prepare the system in the ground state of the XXZ Hamiltonian at parameter Δ_0, and at time $t = 0$ instantaneously quench it from Δ_0 to Δ. We have carried out tDMRG computations for a variety of values of Δ_0 and Δ, and present some representative results in Figs. 21 and 22. The chain length in these simulations is $L = 64$. The initial state is selected by running a static DMRG retaining $\chi_0 = 40$ states. After the quench, we perform the usual time-dependent routine

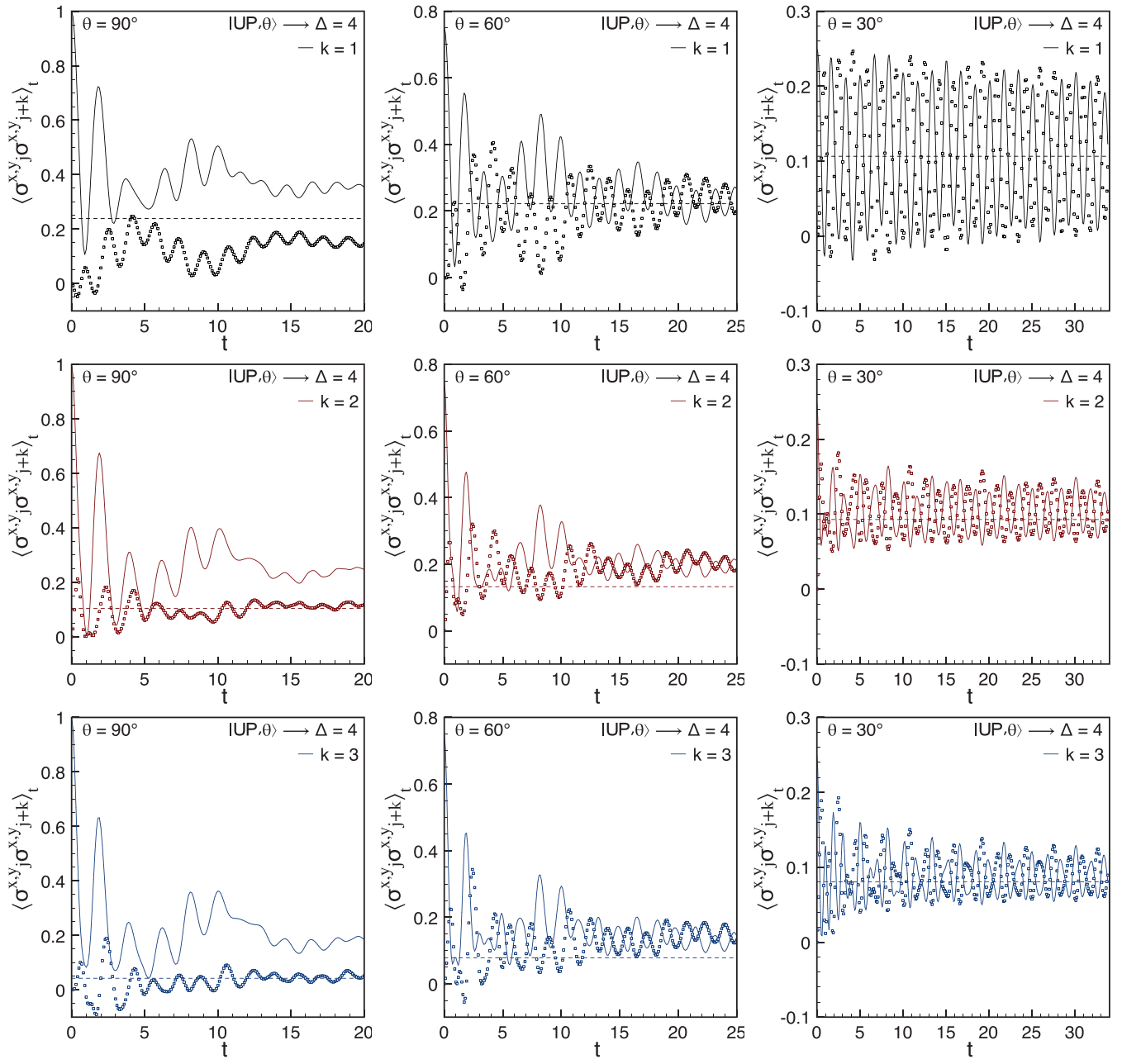

FIG. 18. (Color online) iTEBD results for transverse correlations after a quench from the ferromagnetic state with $\theta = 90°, 60°, 30°$ (from left to right column) to $\Delta = 4$. Solid lines (symbols) correspond to $S^x_{j,j+k}$ ($S^y_{j,j+k}$).

retaining at most $\chi = 300$ states, which is enough to show equilibration because the entanglement entropy grows very slowly (cf. Fig. 8) and so these interaction quenches are less computationally demanding than the quenches out of the initial states we have considered above. It is clear from Figs. 21 and 22 that all correlators relax in an oscillatory way to the GGE predictions (dashed lines) at late times. As in in all previous cases, the principal oscillation has a frequency proportional to Δ, but there are also less important oscillations with higher frequencies. Therefore, for $\Delta = 2$ these oscillations slightly spoil the equilibration around the GGE values on the time scale reported in the figure.

IV. CONCLUSIONS

We have considered quantum quenches from several initial states in the spin-$\frac{1}{2}$ Heisenberg XXZ chain with Ising-type anisotropy $\Delta > 1$. In particular, we considered (a) tilted Néel states; (b) Majumdar-Ghosh dimer product states; (c) tilted ferromagnetic states; and (d) the ground state of the XXZ Hamiltonian for $\Delta_0 > 1$. Following Ref. [8], we constructed the corresponding generalized Gibbs ensembles by means of the quantum transfer-matrix approach. We then determined the short-distance (up to distance three) behavior of spin-spin correlation functions in these ensembles.

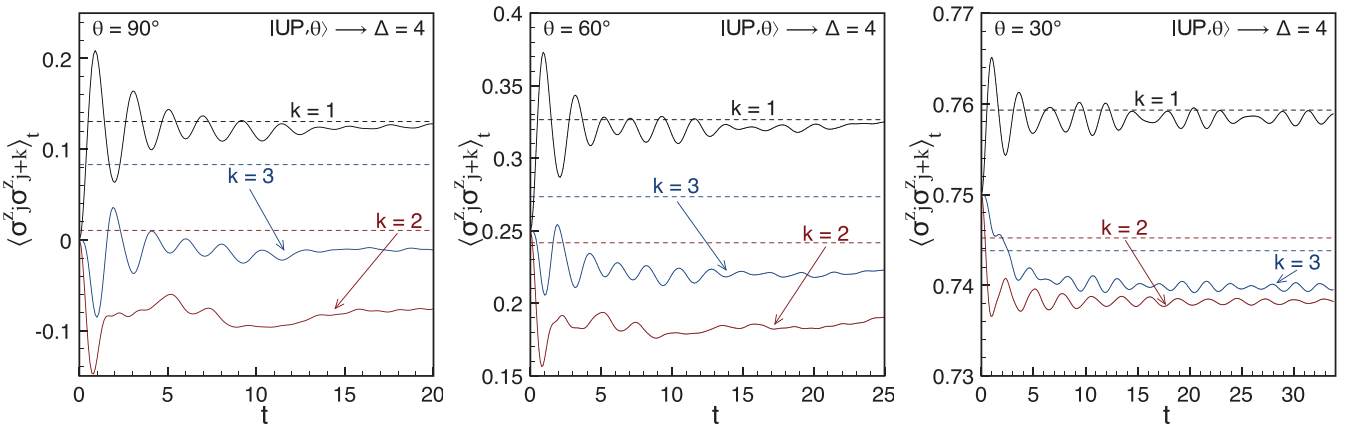

FIG. 19. (Color online) Same as Fig. 18 for longitudinal correlations.

We then considered the time evolution under the XXZ Hamiltonian when starting in these initial states by means of numerical matrix-product techniques (i.e., tDMRG and iTEBD). In cases (a), (b), and (d) we observed that on the accessible time scales, short-distance spin-spin correlators appear to relax towards stationary values, which are in good

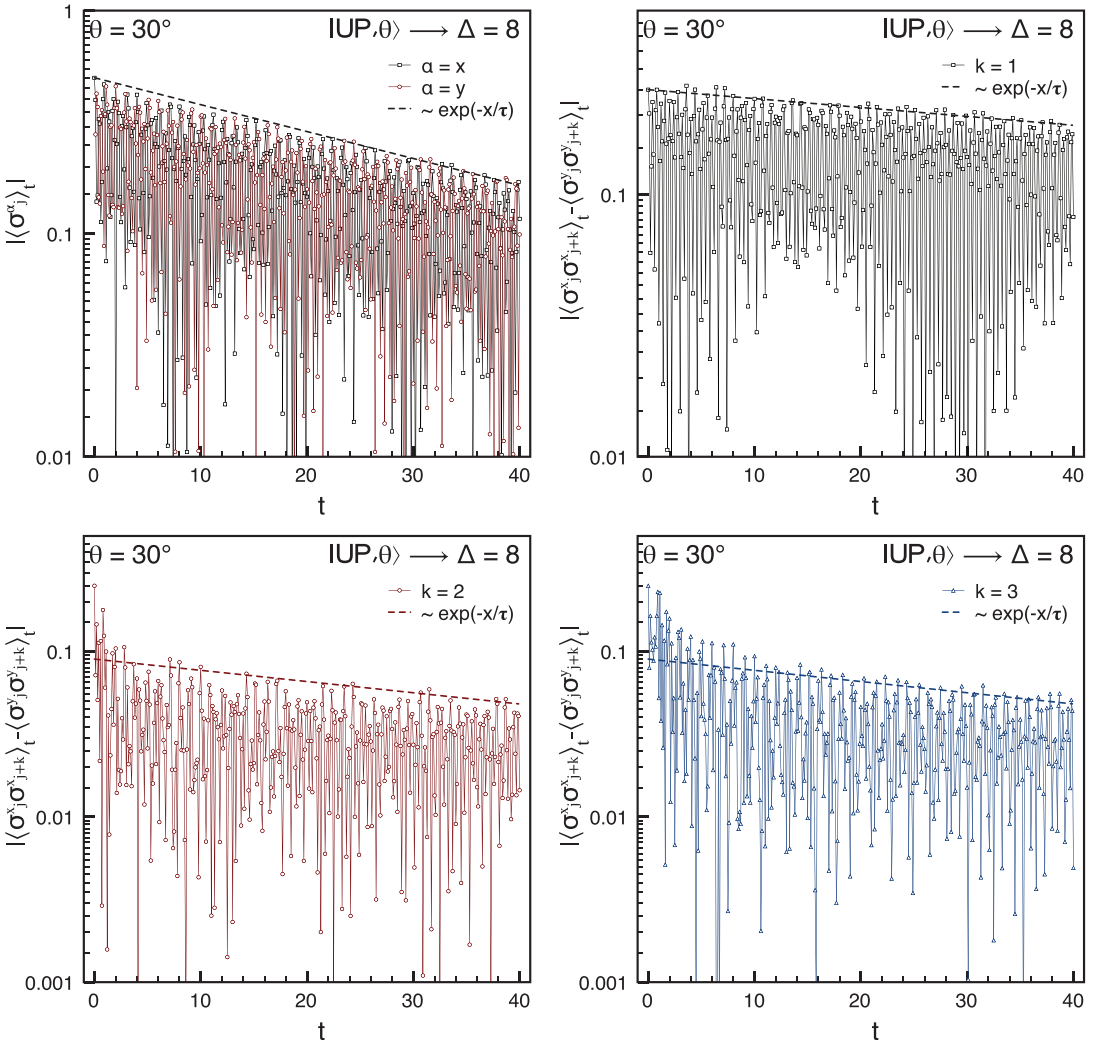

FIG. 20. (Color online) iTEBD results for quenches from the ferromagnetic state with $\theta = 60^\circ$ to $\Delta = 8$. The rightmost panel is the local correlator $\langle\sigma_j^{x,y}\rangle$. The other three panels report the (absolute value of the) difference $|\langle\sigma_j^x\sigma_{j+k}^x\rangle - \langle\sigma_j^y\sigma_{j+k}^y\rangle|$ with $k = 1,2,3$ (going from left to right).

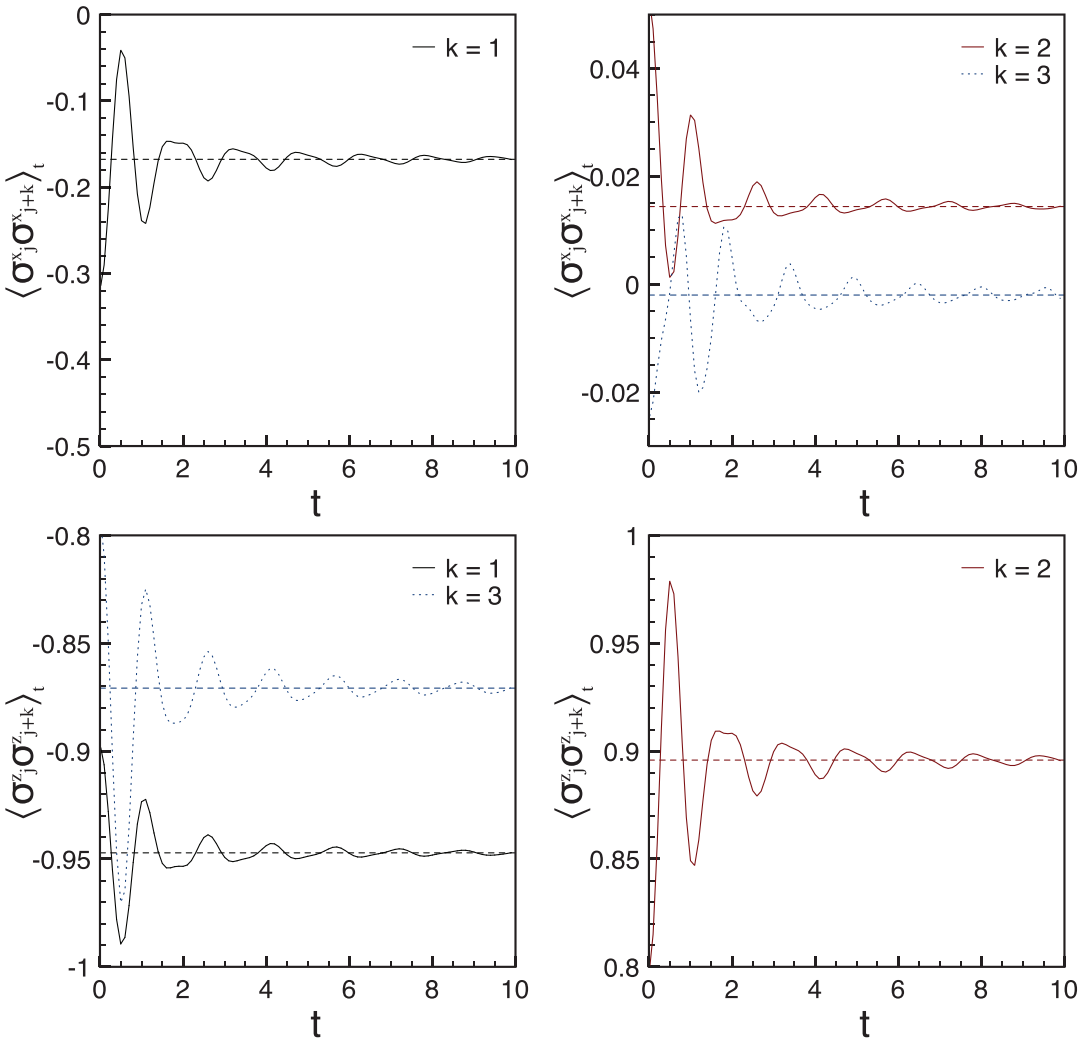

FIG. 21. (Color online) Interaction quenches in the XXZ Hamiltonian from $\Delta_0 = 3$ to $\Delta = 6$. All data are from tDMRG simulations for chains of length $L = 64$.

agreement with the GGE predictions. For tilted ferromagnetic initial states, the presence of an extraordinarily long relaxation time precludes an analysis of the stationary behavior by our numerical methods. First and foremost, these results constitute a strong test of the GGE predictions by independent methods. A second issue we have focused on is that of *symmetry restoration* after quantum quenches. Most of the initial states we considered break symmetries of the XXZ Hamiltonian and the generalized Gibbs ensemble. In order for the GGE to be a valid description of the stationary state at late times, such symmetries must be restored under time evolution. This is indeed what we have observed in our numerical computations. To the best of our knowledge, this phenomenon was previously discussed only for the transverse-field Ising chain [11,12]. Our results for the XXZ chain show the general nature of this phenomenon.

They also raise many interesting open questions and problems:

(i) Our analysis has been restricted to the massive regime $\Delta > 1$. It will be very interesting to extend it to the critical regime $|\Delta| < 1$. For particular choices of initial states, we expect the quasilocal integrals of motion constructed recently [47] to come into play.

(ii) It would be interesting to consider initial states that break the reflection symmetries of the Hamiltonian and lead to GGEs, in which the parity-odd conservation plays a role. In such cases, we expect the reflection symmetry not to be restored at late times.

(iii) We expect symmetry restoration to be a rather generic feature for quenches in one-dimensional systems. This is because spontaneous symmetry breaking may occur only at zero temperature, and the finite-energy density present in the system after a quench plays a role very close to a finite temperature. In higher-dimensional models, it should be possible for spontaneous symmetry breaking to occur in GGEs describing stationary states after quenches. Some similar conclusions on symmetry restoration after a quench were also drawn in Ref. [48] by means of renormalization group arguments and field-theoretical methods (in imaginary time and analytically continuing the final results to real time).

(iv) We have focused on spin-spin correlators on short distances of at most three sites. These can be generalized to

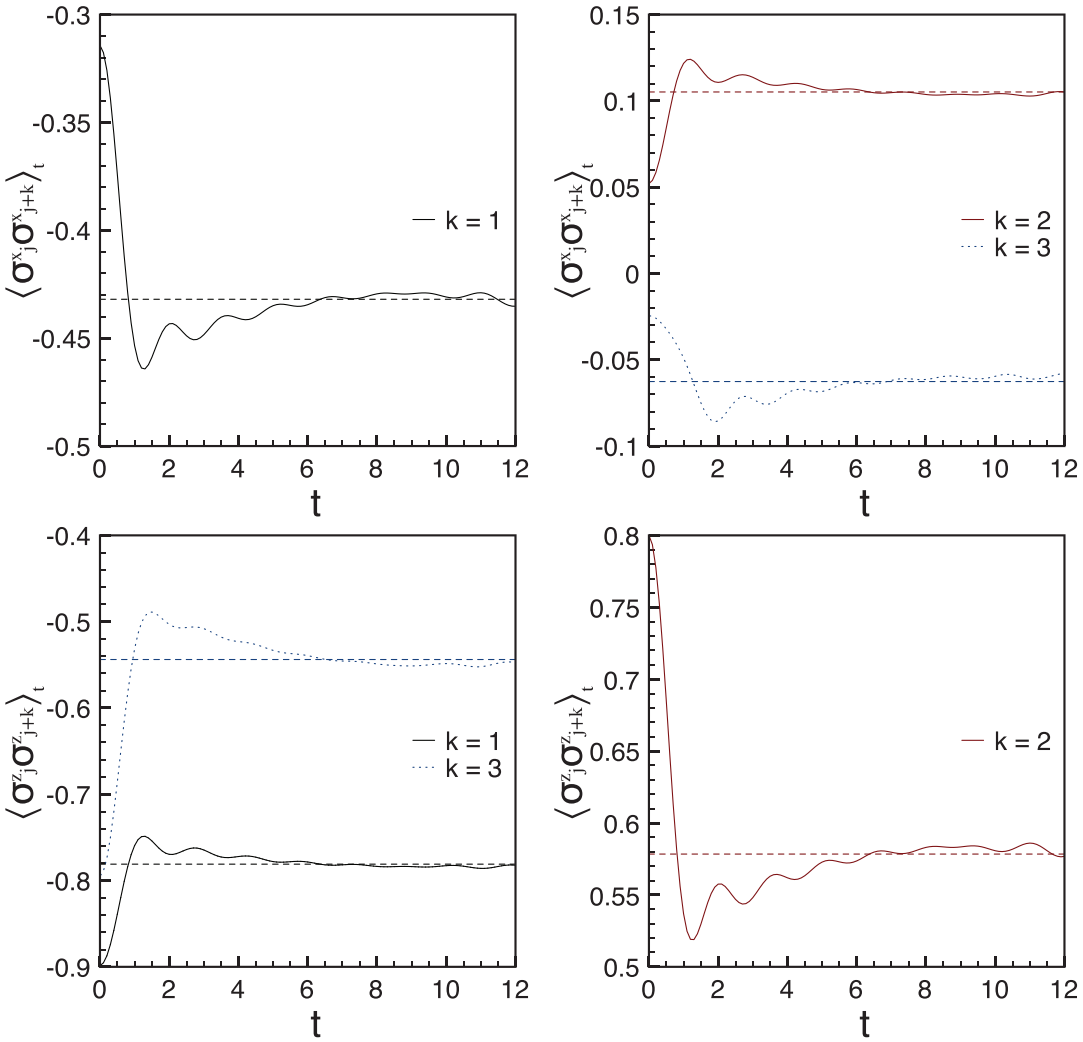

FIG. 22. (Color online) Interaction quenches in the XXZ Hamiltonian from $\Delta_0 = 3$ to $\Delta = 2$. All data are obtained by tDMRG simulations for chains of length $L = 64$.

longer distances by combining the results of Ref. [37] for the thermal case with our formalism of constructing the GGE for a given quench.

(v) Finally, an analytic description of the full time evolution after quantum quenches in interacting integrable models remains a largely open problem. A possible approach to this problem is to use the overlaps between several initial states and arbitrary Bethe states recently reported by Pozsgay [34] to determine the "initial data" in the saddle-point approach of Ref. [29].

An alternative method is based on the Yudson representation [35,49], but at present this is restricted to the limit of zero-energy density (compared to the ground state of the post-quench Hamiltonian). The generalization of this method to finite-energy densities remains an open problem.

ACKNOWLEDGMENT

This work was supported by the EPSRC under Grants No. EP/I032487/1 (F.H.L.E. and M.F.) and No. EP/J014885/1 (F.H.L.E. and M.F.) and by the ERC under Starting Grant No. 279391 EDEQS (P.C. and M.C.).

APPENDIX A: LARGEST EIGENVALUE OF THE QUANTUM TRANSFER MATRIX

In this section, we discuss the validity of some assumptions concerning the leading eigenvalue of our quantum transfer matrix, which underlie the derivation of the system of equations (2.3). The latter was obtained in Ref. [8] by taking the Trotter limit ($N \to \infty$) in the Bethe ansatz equations for the leading eigenvalue of the quantum transfer matrix, which read as

$$\left[\prod_{k=1}^{y} \frac{\sinh\left(w_j - u^{(y)}_{k;N}\right)\sinh(w_j+\eta)}{\sinh\left(w_j - u^{(y)}_{k;N} - \eta\right)\sinh(w_j)}\right]^{N/y} + \prod_{k=1}^{N} \frac{\sinh(w_j - w_k + \eta)}{\sinh(w_j - w_k - \eta)} = 0, \quad j = 1, \ldots, N. \quad \text{(A1)}$$

Here, $u^{(y)}_{k;N}$ are inhomogeneities introduced into the transfer matrix in order for it to give rise to the truncated GGE with only the first y conservation laws retained. The derivation of the integral equations describing the largest eigenvalue

of the quantum transfer matrix was based on the following assumptions:

(a) The thermodynamic limit and the Trotter limit are interchangeable.

(b) The leading eigenvalue of the quantum transfer matrix is nondegenerate and is separated from the subleading eigenvalues by a finite gap.

(c) The largest eigenvalue is determined by a solution of the Bethe ansatz equations with N roots.

In addition, the Trotter limit was taken by assuming that

(d) the solutions of the Bethe ansatz equations for the largest eigenvalue of the quantum transfer matrix lie in the region $\mathrm{Re}[w_j] \in (-\eta/2, \eta/2)$.

The system of equations (2.3) was finally obtained by taking the limit $y \to \infty$. The description of the GGE by considering a limiting procedure in which the number of retained conservation laws is taken to infinity in the end of the calculation was proposed in Ref. [12] and has a sound physical grounding. In the following, we shall accept assumption (a) as it is a central tenet of the quantum transfer-matrix approach, but scrutinize the remaining assumptions for a "truncated GGE"[12] with three conservation laws. For simplicity, we restrict our analysis to parity-invariant initial states, for which the inhomogeneities can be chosen as

$$u^{(3)}_{j;N} = \frac{\sinh\eta}{2}\left(-\lambda_1 \frac{1}{N} + (6\lambda_3)^{1/3}\frac{e^{2\pi i j/3}}{N^{1/3}}\right). \tag{A2}$$

In spite of the unusual dependence on the Trotter number N, the finite-N corrections to the Lagrange multipliers scale as integer powers of $1/N$. It is then reasonable to expect that the role of the small parameter controlling large-N expansions of physical quantities will be played by N^{-1} rather than $N^{-1/3}$. This expectation is borne out by our direct calculations.

The first step in analyzing the spectrum of the transfer matrix is, as always, to identify the root distribution of the leading eigenvalue by comparing the eigenvalues obtained by solving the Bethe ansatz equations (A1) to exact diagonalization data for small system sizes. This analysis shows that for small systems, both (b) and (c) hold. The leading eigenvalue of the transfer matrix is characterized by considering the logarithmic form of the Bethe ansatz equations, which for the quench in Fig. 23 and $N = 0 \bmod 6$ reads as

$$\begin{aligned}\frac{N}{3}\sum_{k=1}^{3}\ln\left(\frac{s_k \sinh\left(w_j - u^{(3)}_{k;N}\right)\sinh(w_j)}{\sinh\left(w_j - u^{(3)}_{k;N} - \eta\right)\sinh(w_j+\eta)}\right)\\ + N\,\ln\left(-\frac{\sinh^2(w_j+\eta)}{\sinh^2(w_j)}\right)\\ + \sum_{k=1}^{N}\ln\left(-\frac{\sinh(w_j - w_k + \eta)}{\sinh(w_j - w_k - \eta)}\right)\\ = 2\pi i I_j,\end{aligned} \tag{A3}$$

where $s_1 = s_2 = -1$ and $s_3 = 1$. The leading eigenvalue of the quantum transfer matrix corresponds to the sequence of half-integer numbers

$$I_j = \frac{1-N}{2}, \ldots, \frac{N-1}{2}. \tag{A4}$$

As usual, we are now able to follow the solution (A4) with increasing N by numerically solving the Bethe ansatz equations (A3). We considered system sizes of a few hundred sites and performed the following checks:

(1) For large N, we checked whether $\mathrm{Re}[w_j] \in (-\eta/2, \eta/2)$.

(2) We extrapolated the leading eigenvalue and the Fourier coefficients of $\rho(x)e^{\zeta(x)/2}$ and compared them with the corresponding quantities obtained from the solution of (2.3) (readapted to the truncated GGE).

Figure 23 shows the Bethe roots w_j that solve (A3) for a rather large value of N for the quench from the ferromagnetic state in the x direction $|{\to}{\to}\ldots\rangle$ with $\Delta = 2$. The roots lie inside the integration contour used to derive the nonlinear integral equations. In addition, the extrapolation of the leading eigenvalue of the quantum transfer matrix in the Trotter limit is in perfect agreement with the value corresponding to the solution of (2.3). An analogous discussion holds true for the Fourier coefficients of $\rho e^{\zeta/2}$, corroborating the assumptions we made.

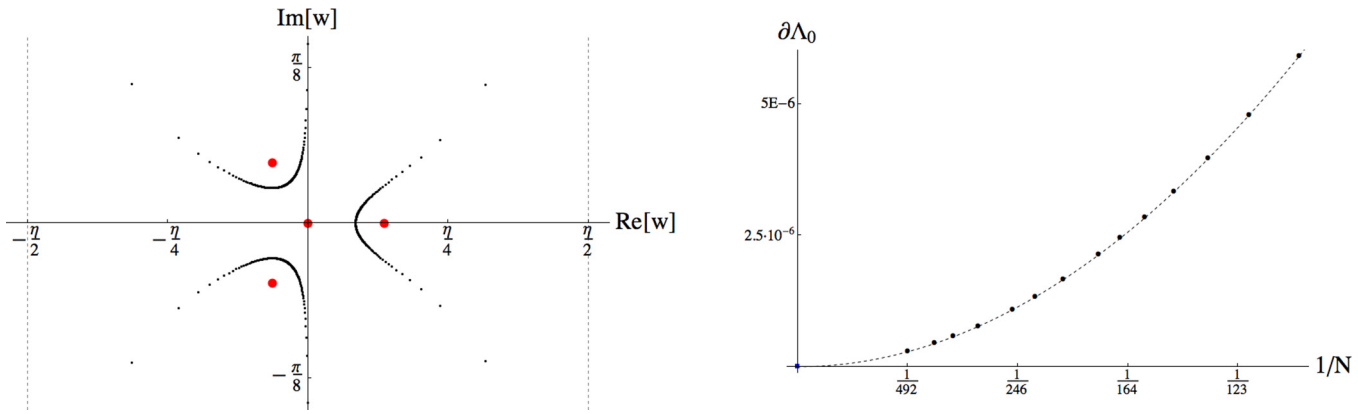

FIG. 23. (Color online) Left: Bethe roots associated with the leading eigenvalue of the quantum transfer matrix for the quench from $|{\to}{\to}\ldots\rangle$ with $\Delta = 2$ and $N = 492$. The dashed lines are part of the contour of integration used to derive the nonlinear integral equations in the Trotter limit. The red points are the inhomogeneities of the transfer matrix, which in the Trotter limit approach 0. Right: The discrepancy $\delta\Lambda(N) \equiv \Lambda_0(N) - \Lambda_0$ between the the largest eigenvalue of the quantum transfer matrix for a finite number of roots and the eigenvalue as computed solving (2.3).

APPENDIX B: LIST OF EXPLICIT RESULTS FOR SPIN-SPIN CORRELATORS IN THE GGE

In this Appendix, we list the GGE results for the spin-spin correlation functions (3.3) calculated by means of the quantum transfer-matrix method as described in the main part of the paper.

			30° Néel			
Δ	F_{x1}	F_{x2}	F_{x3}	F_{z1}	F_{z2}	F_{z3}
2	−0.2951	0.06493	0.002095	−0.5799	0.3076	−0.1919
4	−0.1789	0.02855	0.009815	−0.7231	0.5150	−0.3864
8	−0.09891	0.01684	0.006760	−0.7565	0.5705	−0.4364
			20° Néel			
Δ	F_{x1}	F_{x2}	F_{x3}	F_{z1}	F_{z2}	F_{z3}
2	−0.3194	0.06760	−0.004129	−0.6221	0.3553	−0.2438
4	−0.2000	0.02499	0.004992	−0.8122	0.6526	−0.5552
8	−0.1068	0.008910	0.004371	−0.8709	0.7571	−0.6679
			10° Néel			
Δ	F_{x1}	F_{x2}	F_{x3}	F_{z1}	F_{z2}	F_{z3}
2	−0.3367	0.07108	−0.009721	−0.6482	0.3872	−0.2808
4	−0.2181	0.02592	−0.0005958	−0.8683	0.7483	−0.6845
8	−0.1172	0.007326	0.001055	−0.9443	0.8910	−0.8537
			90° Ferromagnetic			
Δ	F_{x1}	F_{x2}	F_{x3}	F_{z1}	F_{z2}	F_{z3}
4	0.2391	0.1039	0.04256	0.1304	0.01049	0.08296
			60° Ferromagnetic			
Δ	F_{x1}	F_{x2}	F_{x3}	F_{z1}	F_{z2}	F_{z3}
4	0.2219	0.1322	0.07781	0.3266	0.2417	0.2735
			30° Ferromagnetic			
Δ	F_{x1}	F_{x2}	F_{x3}	F_{z1}	F_{z2}	F_{z3}
4	0.1064	0.09290	0.08058	0.7593	0.7452	0.7438
			Majumdar-Ghosh			
Δ	F_{x1}	F_{x2}	F_{x3}	F_{z1}	F_{z2}	F_{z3}
1.2	−0.4799	0.1547	−0.07218	−0.5334	0.2172	−0.1185
1.4	−0.4592	0.1377	−0.05954	−0.5583	0.2531	−0.1428
1.6	−0.4399	0.1240	−0.04998	−0.5751	0.2793	−0.1575
2	−0.4081	0.1042	−0.03752	−0.5919	0.3080	−0.1653
4	−0.3317	0.06584	−0.01802	−0.5842	0.3045	−0.1118
8	−0.2905	0.04834	−0.01067	−0.5524	0.2621	−0.05291
			XXZ ground state: $\Delta_0 = 3$			
Δ	F_{x1}	F_{x2}	F_{x3}	F_{z1}	F_{z2}	F_{z3}
1.25	−0.5102	0.1691	−0.09802	−0.5855	0.2668	−0.1811
1.5	−0.4937	0.1488	−0.09095	−0.6597	0.3725	−0.3010
2	−0.4320	0.1052	−0.06263	−0.7810	0.5784	−0.5439
2.5	−0.3675	0.07300	−0.03914	−0.8560	0.7179	−0.7054
3	−0.3148	0.05235	−0.02452	−0.8981	0.7990	−0.7940
4	−0.2424	0.03031	−0.01032	−0.9344	0.8701	−0.8622
6	−0.1677	0.01440	−0.002004	−0.9472	0.8958	−0.8708

[1] T. Kinoshita, T. Wenger, and D. S. Weiss, Nature (London) **440**, 900 (2006).

[2] S. Trotzky, Y.-A. Chen, A. Flesch, I. P. McCulloch, U. Schollwöck, J. Eisert, and I. Bloch, Nat. Phys. **8**, 325 (2012).

[3] M. Cheneau, P. Barmettler, D. Poletti, M. Endres, P. Schauss, T. Fukuhara, C. Gross, I. Bloch, C. Kollath, and S. Kuhr, Nature (London) **481**, 484 (2012).

[4] M. Gring, M. Kuhnert, T. Langen, T. Kitagawa, B. Rauer, M. Schreitl, I. Mazets, D. A. Smith, E. Demler, and J. Schmiedmayer, Science **337**, 1318 (2012).

[5] U. Schneider, L. Hackermüller, J. P. Ronzheimer, S. Will, S. Braun, T. Best, I. Bloch, E. Demler, S. Mandt, D. Rasch, and A. Rosch, Nat. Phys. **8**, 213 (2012).

[6] J. M. Deutsch, Phys. Rev. A **43**, 2046 (1991); M. Srednicki, Phys. Rev. E **50**, 888 (1994); M. Rigol, V. Dunjko, and M. Olshanii, Nature (London) **452**, 854 (2008); E. Canovi, D. Rossini, R. Fazio, G. Santoro, and A. Silva, New J. Phys. **14**, 095020 (2012).

[7] M. Rigol, V. Dunjko, V. Yurovsky, and M. Olshanii, Phys. Rev. Lett. **98**, 050405 (2007).

[8] M. Fagotti and F. H. L. Essler, J. Stat. Mech. (2013) P07012.

[9] M. Cramer and J. Eisert, New J. Phys. **12**, 055020 (2010).

[10] T. Barthel and U. Schollwöck, Phys. Rev. Lett. **100**, 100601 (2008).

[11] P. Calabrese, F. H. L. Essler, and M. Fagotti, Phys. Rev. Lett. **106**, 227203 (2011); J. Stat. Mech. (2012) P07016; (2012) P07022.

[12] M. Fagotti and F. H. L. Essler, Phys. Rev. B **87**, 245107 (2013).

[13] P. Calabrese and J. Cardy, J. Stat. Mech. (2007) P06008.

[14] A. Iucci and M. A. Cazalilla, Phys. Rev. A **80**, 063619 (2009).

[15] G. Biroli, C. Kollath, and A. M. Läuchli, Phys. Rev. Lett. **105**, 250401 (2010).

[16] D. Fioretto and G. Mussardo, New J. Phys. **12**, 055015 (2010).

[17] F. H. L. Essler, S. Evangelisti, and M. Fagotti, Phys. Rev. Lett. **109**, 247206 (2012).

[18] B. Pozsgay, J. Stat. Mech. (2011) P01011.

[19] A. C. Cassidy, C. W. Clark, and M. Rigol, Phys. Rev. Lett. **106**, 140405 (2011).

[20] M. A. Cazalilla, A. Iucci, and M.-C. Chung, Phys. Rev. E **85**, 011133 (2012).

[21] J.-S. Caux and R. M. Konik, Phys. Rev. Lett. **109**, 175301 (2012).

[22] J.-S. Caux and F. H. L. Essler, Phys. Rev. Lett. **110**, 257203 (2013).

[23] J. Mossel and J.-S. Caux, New J. Phys. **14**, 075006 (2012).

[24] B. Pozsgay, J. Stat. Mech. (2013) P07003.

[25] M. Collura, S. Sotiriadis, and P. Calabrese, Phys. Rev. Lett. **110**, 245301 (2013); J. Stat. Mech. (2013) P09025.

[26] M. Kormos, M. Collura, and P. Calabrese, Phys. Rev. A **89**, 013609 (2014).

[27] G. Mussardo, Phys. Rev. Lett. **111**, 100401 (2013).

[28] J. Mossel and J.-S. Caux, J. Phys. A: Math. Theor. **45**, 255001 (2012); E. Demler and A. M. Tsvelik, Phys. Rev. B **86**, 115448 (2012).

[29] J.-S. Caux and F. H. L. Essler, Phys. Rev. Lett. **110**, 257203 (2013).

[30] J. De Nardis, B. Wouters, M. Brockmann, and J.-S. Caux, arXiv:1308.4310.

[31] M. Kormos, A. Shashi, Y.-Z. Chou, J.-S. Caux, and A. Imambekov, Phys. Rev. B **88**, 205131 (2013).

[32] V. E. Korepin, A. G. Izergin, and N. M. Bogoliubov, *Quantum Inverse Scattering Method, Correlation Functions and Algebraic Bethe Ansatz* (Cambridge University Press, Cambridge, UK, 1993).

[33] M. Fagotti, arXiv:1308.0277; B. Pozsgay, arXiv:1308.3087.

[34] B. Pozsgay, arXiv:1309.4593.

[35] W. Liu and N. Andrei, arXiv:1311.1118.

[36] A. Klümper, Z. Phys. B: Condens. Matter **91**, 507 (1993); C. Destri and H. J. de Vega, Nucl. Phys. B **438**, 413 (1995); A. Klümper and K. Sakai, J. Phys. A: Math. Gen. **35**, 2173 (2002).

[37] H. E. Boos, F. Göhmann, A. Klümper, and J. Suzuki, J. Phys. A: Math. Theor. **40**, 10699 (2007); H. E. Boos, J. Damerau, F. Göhmann, A. Klümper, J. Suzuki, and A. Weiße, J. Stat. Mech. (2008) P08010; C. Trippe, F. Göhmann, and A. Klümper, Eur. Phys. J. B **73**, 253 (2010).

[38] L. Tagliacozzo and A. Ferris (private communication).

[39] A. M. Tsvelik, Phys. Rev. B **42**, 779 (1990); H. Frahm, J. Phys. A: Math. Gen. **25**, 1417 (1992); N. Muramoto and M. Takahashi, J. Phys. Soc. Jpn. **68**, 2098 (1999); A. A. Zvyagin and A. Klümper, Phys. Rev. B **68**, 144426 (2003).

[40] M. Takahashi and M. Suzuki, Prog. Theor. Phys. **48**, 2187 (1972).

[41] M. Fagotti, Phys. Rev. B **87**, 165106 (2013).

[42] S. R. White and A. E. Feiguin, Phys. Rev. Lett. **93**, 076401 (2004); A. J. Daley, C. Kollath, U. Schollwöck, and G. Vidal, J. Stat. Mech. (2004) P04005.

[43] G. Vidal, Phys. Rev. Lett. **98**, 070201 (2007).

[44] P. Calabrese and J. Cardy, J. Stat. Mech. (2005) P04010.

[45] P. Barmettler, M. Punk, V. Gritsev, E. Demler, and E. Altman, Phys. Rev. Lett. **102**, 130603 (2009); New J. Phys. **12**, 055017 (2010).

[46] M. Fagotti, arXiv:1401.1064.

[47] T. Prosen, Phys. Rev. Lett. **106**, 217206 (2011); T. Prosen and E. Ilievski, *ibid*. **111**, 057203 (2013).

[48] A. Gambassi and P. Calabrese, Europhys. Lett. **95**, 66007 (2011).

[49] A. Lamacraft, Phys. Rev. A **84**, 043632 (2011).